ISSN 0869-5911, Petrology, 2006, Vol. 14, No. 5, pp. 492–514. © Pleiades Publishing, Inc., 2006.
Original Russian Text © A.V. Girnis, V.K. Bulatov, Y. Lahaye, G.P. Brey, 2006, published in Petrologiya, 2006, Vol. 14, No. 5, pp. 524–547.

# Partitioning of Trace Elements between Carbonate–Silicate Melts and Mantle Minerals: Experiment and Petrological Consequences

**A. V. Girnis[a], V. K. Bulatov[b], Y. Lahaye[c], and G. P. Brey[c]**

[a] *Institute of Geology of Ore Deposits, Petrography, Mineralogy, and Geochemistry (IGEM), Russian Academy of Sciences, Staromonetnyi per. 35, Moscow, 109017 Russia*
*e-mail: girnis@igem.ru*

[b] *Vernadsky Institute of Geochemistry and Analytical Chemistry, Russian Academy of Sciences, ul. Kosygina 19, Moscow, 119991 Russia*

[c] *Institut für Mineralogie, J.-W.-Goethe-Universität Frankfurt am Main, Senckenberganlage 28, 60054 Frankfurt/M, Germany*

Received September 10, 2005

**Abstract**—The partitioning of a number of trace elements (Ba, Nb, Zr, Y, REE, etc.) between orthopyroxene, garnet, and carbonate–silicate melt was experimentally studied using a belt apparatus at pressures of 3.5–4.2 GPa and temperatures of 1300–1500°C. The experimental products were investigated by electron microprobe analysis and laser ablation inductively coupled plasma mass spectrometry (LA-ICP-MS). The experimental melts varied from carbonatitic (~5 wt % $SiO_2$) at low temperatures (1300–1350°C) to kimberlitic compositions (30 wt % $SiO_2$) at high temperatures (1500°C). The partition coefficients of most elements between orthopyroxene and melt ($D_i^{Opx/L}$) and garnet and melt ($D_i^{Grt/L}$) were almost independent of melt composition (temperature). The $D_i^{Opx/L}$ values ranged from <0.01 for the most incompatible Ba and light REE to 0.02–0.08 for moderately incompatible Zr, Y, and heavy REE. The $D_i^{Grt/L}$ values were approximately an order of magnitude higher, ~0.07 for light REE, 0.7 for Y, and 1.5 for Yb. The character of $D_i^{Grt/L}$ variations in the systems studied is in general similar to that established for silicate melts without volatile components. However, the differences in the behavior of moderately incompatible and compatible elements (e.g., light and heavy REE) in the experimental systems are less pronounced compared with $CO_2$-free systems. Considering carbonate–silicate and silicate melts as possible agents of mantle metasomatism, it can be concluded that the former can efficiently transport heavy REE, and the latter have a greater affinity for Nb, Ba, and light REE. A characteristic feature of mantle rocks enriched by carbonate–silicate melts is high Ba/La ratio coupled with relatively weakly fractionated REE distribution patterns. It was shown that the high degrees of enrichment observed in natural kimberlites can be explained by a two-stage scenario, including a preliminary invasion of carbonate–silicate melt into depleted harzburgites in the lower parts of the lithosphere and subsequent very low degree melting.

**DOI:** 10.1134/S0869591106050055

## INTRODUCTION

Kimberlitic melts are the deepest magmas transported from the mantle into upper crustal levels. The available experimental and geochemical data suggest that primary kimberlite magmas could be derived by the melting of $CO_2$-bearing mantle peridotites at a pressure of no less than 5 GPa (e.g., Eggler, 1989; Wyllie, 1989). Experimental studies have shown that near-solidus melts formed in a carbonated peridotite at pressures of more than 3 GPa have carbonatite compositions (Wallace and Green, 1988; Ryabchikov et al., 1989; Dalton and Wood, 1993; Dalton and Presnall, 1998). Melts with very high $CO_2$ contents can be generated not only in a carbonated material but also in the primitive or even depleted mantle at very low degrees of melting (Ryabchikov, 2003). Such melts may serve as agents of mantle metasomatism (Green and Wallace; Hunter and McKenzie, 1989). At pressures above 3 GPa, the carbonate melts from a carbonated peridotite gradually change with increasing temperature to kimberlitic compositions (Ryabchikov et al., 1993; Moore and Wood, 1998; Dalton and Presnall, 1998; Girnis et al., 2005). Note that all these melts can be regarded as near-solidus liquids in the sense that they are formed at very low degrees of melting, although the temperature difference between carbonate and kimberlite melts may be as high as hundreds of degrees (e.g., Moore and Wood, 1998).

Thus, the problem of kimberlite magma genesis is closely interwoven with the role of carbonate melts in the mantle. Carbonate melts from deep mantle zones can produce kimberlite magmas with specific geochemical signatures during ascent and decompression. The modeling of geochemical effects related to the migration of carbonate and carbonate–silicate melts in the mantle and their interaction with mantle rocks requires knowledge of trace-element partition coefficients between these melts and mantle minerals at high pressures. In recent years limited experimental data have been obtained on trace element partitioning in the systems carbonate melt–minerals (Sweeney, 1994; Sweeney et al., 1992, 1995; Klemme et al., 1995; Blundy and Dalton, 2000; Adam and Green, 2001) under mantle parameters. Keshav et al. (2005) investigated trace element partitioning between a model kimberlite melt and clinopyroxene at 6 GPa and 1410–1430°C. The experiments showed that the partition coefficients of trace and major elements in such systems may be sensitive to variations in pressure, temperature, and melt composition (Blundy and Dalton, 2000; Keshav et al., 2005; Girnis et al., 2005). Because of this, the use of partition coefficients obtained in carbonate or volatile-free silicate systems for modeling equilibria with kimberlite (carbonate–silicate) melts may be misleading. In addition, the aforementioned studies focused mainly on clinopyroxene–melt partitioning, whereas many kimberlite melts are probably related to the melting of clinopyroxene-free source materials (Girnis et al., 1995). With these considerations in mind, we undertook an experimental study of trace element partitioning in the systems carbonate melt–orthopyroxene–garnet and kimberlite melt–orthopyroxene–garnet at pressures of 3.5–4.0 GPa under $CO_2$-saturated conditions.

## METHODS

### *Starting Materials*

The compositions of starting materials were similar to those used in our previous experiments on the crystallization of $CO_2$-saturated kimberlitic melt under mantle conditions (Girnis et al., 2005). The mixtures from this study differed in that varying amounts of trace elements were added, and the range of CaO contents was wider, from 2 to more than 20 wt % (Table 1), which was aimed at exploring the possible influence of Ca on trace-element partitioning. The concentration of CaO in mix KMg2Tnat approximately corresponded to the average composition of group IA kimberlites (Smith et al., 1985). The garnets and orthopyroxenes that crystallized from this composition showed moderate CaO contents, significantly lower than in the minerals coexisting with clinopyroxene. In order to obtain clinopyroxene-saturated melts, a mix with 20 wt % of additional calcite was prepared (KCaCO3Tnat). This composition yielded the equilibrium clinopyroxene–orthopyroxene–garnet assemblage in experiments.

Since one of the goals of this study was the development of analytical methods for the analysis of quench aggregates, initial mixes with different contents of trace elements were prepared. Mix KCa3T05 contained approximately 0.5 wt % of $ZrO_2$, $Nb_2O_5$, $Sc_2O_3$, $La_2O_3$, and $Yb_2O_3$ and was aimed at checking the accuracy of the concentrations of these elements in quenched carbonate–silicate melts determined by LA-ICP-MS by comparing with the results of electron microprobe analysis. The other mixes contained small amounts (50–150 ppm) of a number of trace elements (Table 1).

The starting materials were prepared from high-purity or reagent-grade $SiO_2$, $TiO_2$, $Al_2O_3$, $Fe_2O_3$, $Ca_3PO_4$, $Na_2CO_3$, and $K_2CO_3$. Trace elements were introduced either as oxides (mix KCa3T05) or as a preliminarily prepared potassium-rich siliceous glass containing tenths of a weight percent of each trace element. These materials were mixed in the desired proportions and were annealed at 1150°C in a graphite crucible. After this, Ca and Mg carbonates were added to the mixtures. The mixtures were ground under acetone in an agate mortar for 2 h and stored at a temperature of about 100°C.

### *Experimental Procedure*

The starting material was loaded into a graphite container and welded shut in an outer thick-wall (0.2 mm wall thickness) platinum capsule with an inner diameter of 4 mm and a height of 3 mm. The experiments were carried out on a belt apparatus (Brey et al., 1990) at the Institute of Mineralogy, Frankfurt am Main, Germany. The solid-phase cell assembly of the belt apparatus consists of a graphite heater and sleeves and cylinders manufactured from natural polycrystalline fluorite. Temperature was measured and controlled during experiments by a $PtRh_6$–$PtRh_{30}$ thermocouple. Pressure was calibrated under high temperatures using the quartz–coesite, diamond–graphite, and fayalite–spinel phase transitions. The accuracy of the determination of experimental parameters was ±0.3 GPa and ±15°C (Brey et al., 1990). During the initial phase of experiments, pressure was increased at ambient temperature, after which temperature was raised at a rate of 50°C/min. In order to increase the size of crystal phase, a two-step heating schedule was employed in several experiments. Temperature was initially raised about 50°C above the desired value. The sample was kept under such conditions for 0.5 h, after which temperature was decreased to the desired value at a rate of 10°C/min. The duration of experiments depended on the final temperature. It should be noted that the two-step heating did not result in any significant increase in the size of crystals, and most experiments were therefore conducted without preliminary overheating. The samples were quenched at a rate of about 200°C/s by shutting off the electric power. After experiments, samples were removed from the capsules, mounted in epoxy, and polished for subsequent analysis.

**Table 1.** Chemical compositions of the starting materials used in experiments

| Component | KCa3T0.5 | KCa1Tnat | KCa3Tnat | KMg2Tnat | KCaCO3Tnat |
|---|---|---|---|---|---|
| $SiO_2$, wt % | 34.98 | 39.18 | 34.24 | 33.57 | 31.02 |
| $TiO_2$ | 1.86 | 2.15 | 1.90 | 1.78 | 1.65 |
| $Al_2O_3$ | 3.30 | 3.70 | 3.10 | 3.18 | 2.94 |
| FeO | 9.72 | 10.89 | 9.92 | 9.32 | 8.62 |
| MgO | 33.04 | 38.80 | 33.79 | 41.8 | 30.21 |
| CaO | 14.26 | 2.20 | 14.55 | 8.13 | 23.51 |
| $Na_2O$ | 0.19 | 0.21 | 0.19 | 0.18 | 0.17 |
| $K_2O$ | 0.95 | 1.06 | 0.76 | 0.91 | 0.84 |
| $P_2O_5$ | 0.95 | 1.06 | 0.97 | 0.91 | 0.84 |
| $Cr_2O_3$ | 0.23 | 0.23 | 0.23 | 0.22 | 0.20 |
| NiO | 0.14 | 0.14 | 0.14 | – | – |
| BaO | 0.24 | 0.24 | 0.06 | – | – |
| SrO | 0.14 | 0.14 | 0.14 | – | – |
| Total | 100.00 | 100.00 | 100.00 | 100.00 | 100.00 |
| $CO_2$ | 31.00 | 31 | 31.00 | 34 | 34 |
| Li, ppm | – | 40 | 100 | 100 | 100 |
| Sc | 3260 | 20 | 50 | 50 | 50 |
| V | – | 120 | 300 | 300 | 300 |
| Co | – | 85 | 250 | 220 | 220 |
| Zn | – | 65 | 200 | 160 | 160 |
| Rb | – | 60 | 200 | 150 | 150 |
| Sr | 1184 | 1184 | 1184 | – | – |
| Y | – | 50 | 150 | 125 | 125 |
| Zr | 3700 | 250 | 500 | 625 | 625 |
| Nb | 3500 | 160 | 400 | 400 | 400 |
| Ba | 2150 | 2150 | 500 | – | – |
| La | 4260 | 140 | 500 | 350 | 350 |
| Ce | – | 240 | 500 | 600 | 600 |
| Pr | – | 80 | 400 | 200 | 200 |
| Nd | – | 95 | 400 | 240 | 240 |
| Sm | – | 50 | 200 | 125 | 125 |
| Eu | – | 50 | 200 | 125 | 125 |
| Gd | – | 50 | 200 | 125 | 125 |
| Tb | – | 50 | 200 | 125 | 125 |
| Dy | – | 50 | 200 | 125 | 125 |
| Ho | – | 50 | 200 | 125 | 125 |
| Er | – | 50 | 200 | 125 | 125 |
| Tm | – | 50 | 200 | 125 | 125 |
| Yb | 4390 | 50 | 200 | 125 | 125 |
| Lu | – | 50 | 200 | 125 | 125 |
| Hf | – | 50 | 200 | 125 | 125 |
| Ta | – | 50 | 200 | 125 | 125 |
| Pb | – | 15 | 200 | 40 | 40 |

### *Analytical Techniques*

The concentrations of major elements in experimental products were determined using a JEOL Superprobe 8900 electron microprobe equipped with five spectrometers (Institute of Mineralogy, J.-W.-Goethe University, Frankfurt am Main, Germany). The analytical conditions were 20 kV accelerating voltage, 20 nA beam current, and peak and background counting times of 20–40 s and 10–20 s, respectively. Minerals were analyzed with a focused beam (beam excitation volume is about 2 μm in diameter), and the products of melt quenching were analyzed with a defocused beam, 20–30 μm in diameter. Quench orthopyroxene and carbonates were often comparable in size with the beam diameter (30–50 μm long and up to 10 μm wide) (Fig. 1). The microprobe analyses of such aggregates are characterized by a considerable scatter. Our previous studies (Girnis et al., 2005) showed that the average compositions of such aggregates become stable when the number of microprobe measurements is no less than 10–30, depending on the size of quench crystals. Therefore, quenched melts were analyzed in at least 15 spots, and up to 40 measurements were conducted in samples with the largest quench crystals. Oxides, silicates, and metals provided by JEOL were used as standards. The characteristic X-ray intensities were recalculated to concentrations using the ZAF program.

Trace elements were analyzed by laser ablation inductively coupled plasma mass spectrometry (LA-ICP-MS) at the Institute of Mineralogy, Frankfurt am Main. The instrument consists of an UV Nd-YAG laser probe (Merchantek LUV213) and a Finnigan MAT ELEMENT 2 mass spectrometer. The analytical procedure was described in detail by Lahaye et al. (1997). Synthetic glasses (NIST 610) were used as standard. The concentrations were calculated by normalizing to the Ca content measured on the electron microprobe. The accuracy of concentrations was mostly about 5% (1σ).

## EXPERIMENTAL RESULTS

The conditions of experiments and the phase compositions of experimental products are given in Table 2.

### *Phase Composition*

Phase relationships in the experimental products are consistent with the results of our previous studies of the behavior of major elements in kimberlite systems (Girnis et al., 1995, 2005). Orthopyroxene is the liquidus mineral at pressures of about 4 GPa, and garnet appears as temperature decreases. Most of the experimental products contained a quenched carbonate–silicate melt coexisting with orthopyroxene and garnet (Fig. 1a). Gas bubbles were observed in almost all experiments, which suggests that the melt was saturated in $CO_2$. Gas was absent only in run KTr2, the products of which contained olivine. In this experiment, the capsule probably leaked, and part of $CO_2$ escaped, which resulted in the expansion of the olivine stability field. Nonetheless, $CO_2$ activity was high even in this experiment, which is indicated by the abundance of quench carbonates. Cli-

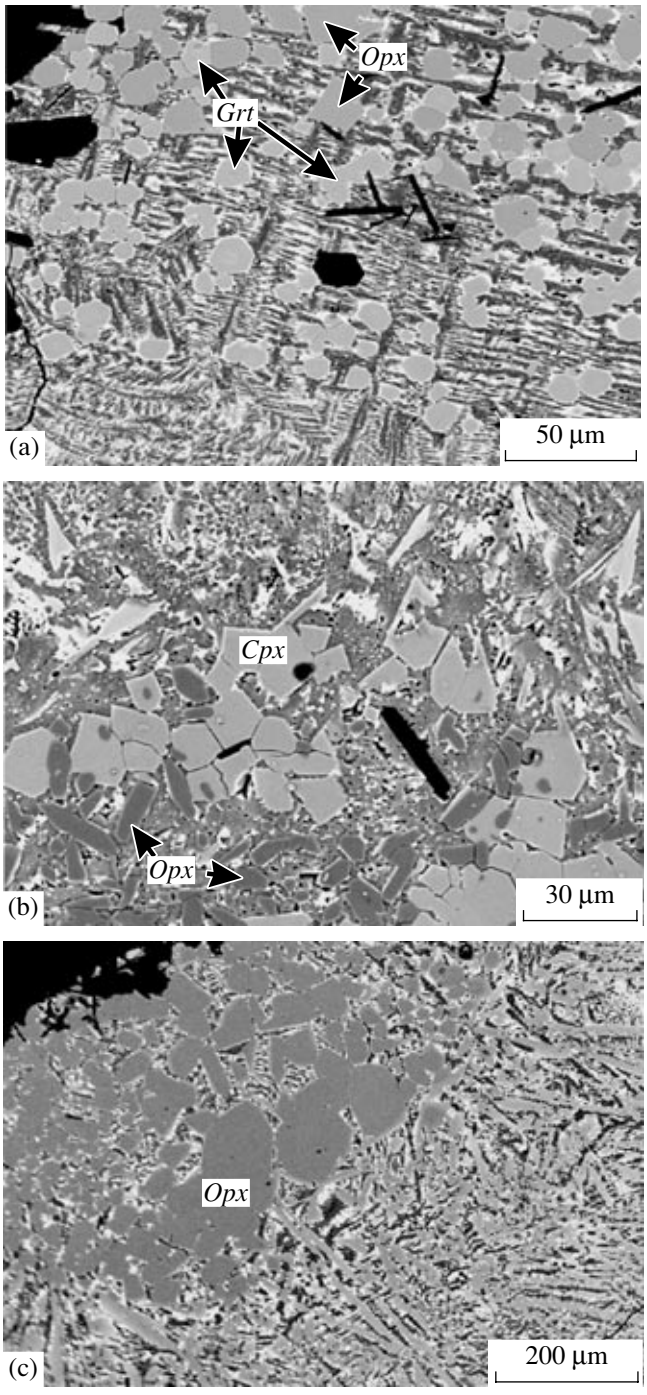


**Fig. 1.** Back-scattered electron images of experimental products. (a) Run KTr10, 4.1 GPa, 1400°C; equilibrium orthopyroxene and garnet crystals in a quench aggregate. (b) Run KTr12, 4.1 GPa, 1400°C; clinopyroxene and orthopyroxene crystals in a quench aggregate. (c) Run KTr11, 4.1 GPa, 1500°C; very large orthopyroxene crystals in a quench aggregate.

**Table 2.** Run conditions and phase compositions of experimental products

| Run no. | Starting mix | *P*, GPa | *T*, °C | Duration, h | Products** |
|---|---|---|---|---|---|
| KTr-1 | KCa3T0.5 | 4 | 1530–>1500* | 30 | *Opx*, *Grt*, *L*, *F* |
| KTr-2 | KCa3T0.5 | 3.5 | 1450–>1400* | 73 | *Opx*, *Ol*, *Grt*, *L* |
| KTr-3 | KCa3T0.5 | 3.5 | 1380 | 77 | *Opx*, *Grt*, *L*, *F* |
| KTr-4 | KCa3T0.5 | 4.1 | 1420 | 48.5 | *Opx*, *Grt*, *L*, *F* |
| KTr-5 | KCa1Tnat | 3.6 | 1360 | 76 | *Opx*, *Grt*, *L*, *F* |
| KTr-6 | KCa1Tnat | 3.6 | 1350–>1300* | 75 | *Opx*, *Grt*, *L*, *F* |
| KTr-7 | KCa1Tnat | 4.15 | 1450 | 48 | *Opx*, *Grt*, *L*, *F* |
| KTr-8 | KCa3Tnat | 4.2 | 1430–>1380* | 72 | *Opx*, *L*, *F* |
| KTr-10 | KMg2Tnat | 4.1 | 1400 | 120 | *Opx*, *Grt*, *L*, *F* |
| KTr-11 | KMg2Tnat | 4.1 | 1500 | 48 | *Opx*, *L*, *F* |
| KTr-12 | KCaCO3Tnat | 4.1 | 1400 | 48 | *Opx*, *Grt*, *Cpx*, *L* |
| KTr-13 | KCaCO3Tnat | 3.5 | 1350 | 93 | *Opx*, *Grt*, *Cpx*, *L* |
| KTr-15 | KCaCO3Tnat | 4 | 1350 | 118 | *Opx*, *Grt*, *Cpx*, *L* |

* Two-stage heating procedure was used with a preliminary exposure at the higher temperature for 0.5–1.0 h.
** Phase abbreviations: *Opx*, orthopyroxene; *Cpx*, clinopyroxene; *Grt*, garnet; *Ol*, olivine; *L*, quenched melt; and *F*, $CO_2$ fluid.

nopyroxene coexisting with orthopyroxene and garnet (Fig. 1b) was observed in experiments KTr12, KTr13, and KTr15 with high calcite content.

The reliable analysis of trace elements in silicates by LA-ICP-MS requires crystalline phases larger than 20 μm. As was mentioned above, our attempts to grow large crystals by two-step heating were not very successful. Large orthopyroxene crystals were obtained in many experiments (up to 100–200 μm, Fig. 1c). In most cases, garnet was smaller than 15 μm (Fig. 1a), and trace elements were analyzed in garnet only in a few samples. Clinopyroxene crystals from the experiments with excess calcite in the initial mixture were also not large enough for the LA-ICP-MS method (Fig. 1b). The analysis of grains about 10 μm in size resulted in significant contamination by the material of the surrounding quench aggregate and too high partition coefficients for incompatible elements. Because of this, trace element partitioning between clinopyroxene and melt was characterized using the data of electron microprobe analysis only.

### *Compositions of Experimental Products: Major Elements*

The compositions of minerals and melts vary regularly depending on experimental conditions (Table 3), and the observed trends are consistent with the results of our previous experiments (Girnis et al., 1995, 2005). The concentration of MgO in orthopyroxene decreases and those of FeO and $TiO_2$ increase as temperature decreases from 1500 to 1300°C (Fig. 2). The concentrations of $Al_2O_3$ and $Cr_2O_3$ are almost invariant, owing to the buffering influence of the coexisting garnet. Variations in CaO concentration are mainly due to the considerable differences in CaO content between the starting materials. Orthopyroxene from the experiments with the addition of calcite contains about 2 wt % CaO, which is the maximum CaO content of orthopyroxene in equilibrium with clinopyroxene. These data are in agreement with the experimental compositions of pyroxenes obtained under similar conditions in simple systems (Nickel and Brey, 1984). In all other experiments, the abundance of CaO in orthopyroxene was much lower (<1 wt %).

Variations in garnet composition in the experimental products are shown in Fig. 3. The concentrations of $TiO_2$ and $Al_2O_3$ show minor variations. The concentration of FeO increases significantly and that of $Cr_2O_3$ declines with decreasing temperature. Similar to orthopyroxene, the CaO content of garnet is controlled by the composition of the starting material and reaches 5–6 wt % in garnet coexisting with clinopyroxene. In all other experiments, garnet contains less than 3 wt % CaO.

Clinopyroxene was analyzed only in three experiments (3.5–4.1 GPa and 1350–1400°C). Its composition (Table 3) corresponds to subcalcic augite (12–16 wt % CaO). The concentration of $Al_2O_3$ is rather stable (2–3 wt %), and the grains are usually homogeneous. The concentrations of minor elements (Na, Cr, and Ti) lie within the range 0.2–0.3 wt %.

The compositions of melts (Fig. 4) change systematically with decreasing temperature from kimberlitic at 1500°C (25 wt % $SiO_2$, which is close to the starting material) to carbonatitic (about 5 wt % $SiO_2$) at 1300°C. The depletion of $Al_2O_3$ and $Cr_2O_3$ in the melt (Fig. 4) is controlled by the crystallization of orthopyroxene and garnet. The concentrations of other elements are more strongly dependent on the composition of the starting material, which can be illustrated by the

**Table 3.** Electron microprobe analyses of experimental phases, wt %

| Component | KTr-1* | | | KTr-2 | | | | KTr-3 | | |
|---|---|---|---|---|---|---|---|---|---|---|
| | *L*** | *Opx* | *Grt* | *L* | *Opx* | *Grt* | *Ol* | *L* | *Opx* | *Grt* |
| | 35*** | 14 | 11 | 40 | 7 | 12 | 8 | 60 | 18 | 12 |
| $SiO_2$ | 19.7(1) | 56.1(3) | 41.7(1) | 17.8(9) | 55.2(3) | 41.2(2) | 40.4(1) | 10.9(8) | 55.5(3) | 41.04(10) |
| $TiO_2$ | 1.84(6) | 0.15(2) | 0.40(5) | 2.02(10) | 0.24(1) | 0.47(8) | 0.02(1) | 2.26(11) | 0.32(5) | 0.6(1) |
| $Al_2O_3$ | 2.21(10) | 2.6(2) | 21.1(3) | 2.01(11) | 3.2(2) | 21.3(3) | 0.11(2) | 1.06(8) | 2.6(3) | 21.1(3) |
| $Cr_2O_3$ | 0.18(2) | 0.37(3) | 1.81(7) | 0.15(2) | 0.44(4) | 1.80(8) | 0.08(1) | 0.11(2) | 0.30(3) | 1.62(7) |
| FeO | 6.95(15) | 4.83(6) | 5.38(7) | 7.2(2) | 5.01(5) | 5.38(4) | 8.06(7) | 7.08(15) | 5.90(8) | 6.55(6) |
| MgO | 22.8(2) | 35.3(2) | 24.2(2) | 21.9(5) | 34.8(2) | 23.7(2) | 51.6(2) | 20.8(2) | 34.6(3) | 23.1(1) |
| CaO | 15.1(3) | 0.92(5) | 2.63(8) | 16.8(4) | 0.90(5) | 2.91(7) | 0.14(2) | 19.2(3) | 0.84(7) | 2.94(7) |
| $Na_2O$ | 0.43(5) | 0.05(1) | 0.02(1) | 0.49(7) | 0.04(1) | 0.00 | 0.00 | 0.50(3) | 0.04(1) | 0.03(1) |
| $K_2O$ | 0.96(15) | 0.00 | 0.00 | 1.01(15) | 0.00 | 0.00 | 0.00 | 1.3(1) | 0.00 | 0.00 |
| $P_2O_5$ | 0.7(1) | 0.00 | 0.02(1) | 0.79(9) | 0.00 | 0.02(1) | 0.00 | 0.95(9) | 0.00 | 0.03(1) |
| $ZrO_2$ | 0.69(4) | 0.00 | 0.24(3) | 0.73(6) | 0.00 | 0.31(4) | 0.00 | 0.6(5) | 0.00 | 0.27(3) |
| SrO | 0.19(3) | 0.00 | 0.00 | 0.22(3) | 0.00 | 0.00 | 0.00 | 0.25(4) | 0.00 | 0.00 |
| $Yb_2O_3$ | 0.54(2) | 0.00 | 0.9(1) | 0.59(4) | 0.00 | 1.24(8) | 0.03(1) | 0.64(4) | 0.02(2) | 1.2(1) |
| $La_2O_3$ | 0.51(5) | 0.00 | 0.00 | 0.64(4) | 0.00 | 0.00 | 0.00 | 0.75(6) | 0.00 | 0.00 |
| $Sc_2O_3$ | 0.50(2) | 0.12(1) | 1.44(7) | 0.50(1) | 0.21(2) | 1.71(6) | 0.05(1) | 0.48(2) | 0.18(2) | 1.77(9) |
| Total | 73.3(7) | 100.44(40) | 99.84(25) | 72.85(120) | 100.04(23) | 100.04(36) | 100.49(25) | 66.88(87) | 100.30(25) | 100.25(18) |

| Component | KTr-4 | | | KTr-5 | | | KTr-6 | | |
|---|---|---|---|---|---|---|---|---|---|
| | *L* | *Opx* | *Grt* | *L* | *Opx* | *Grt* | *L* | *Opx* | *Grt* |
| | 35 | 9 | 12 | 40 | 24 | 14 | 17 | 14 | 4 |
| $SiO_2$ | 12.0(8) | 55.8(3) | 41.3(3) | 15.9(16) | 55.1(4) | 42.4(5) | 5.9(9) | 55.0(3) | 41.5(3) |
| $TiO_2$ | 2.3(1) | 0.27(4) | 0.6(1) | 2.1(2) | 0.29(3) | 0.7(1) | 2.1(5) | 0.51(6) | 1.3(4) |
| $Al_2O_3$ | 1.21(9) | 2.4(1) | 20.7(5) | 2.0(2) | 3.3(4) | 21.8(5) | 0.6(2) | 2.7(3) | 21.5(4) |
| $Cr_2O_3$ | 0.06(6) | 0.29(2) | 1.57(10) | 0.06(2) | 0.34(4) | 1.34(7) | 0.01(1) | 0.25(3) | 1.1(3) |
| FeO | 7.1(1) | 5.72(5) | 6.48(7) | 7.3(3) | 5.6(1) | 6.32(8) | 6.9(5) | 6.7(1) | 7.86(8) |
| MgO | 20.9(3) | 34.8(1) | 23.3(1) | 22.4(5) | 35.0(3) | 24.6(3) | 20.2(9) | 34.6(2) | 23.1(1) |
| CaO | 18.2(3) | 0.89(5) | 3.1(2) | 2.84(9) | 0.14(1) | 0.46(2) | 3.4(2) | 0.13(1) | 0.5(5) |
| $Na_2O$ | 0.53(5) | 0.05(1) | 0.04(1) | 0.37(10) | 0.03(1) | 0.00 | 0.8(4) | 0.04(1) | 0.03(1) |
| $K_2O$ | 0.2(1) | 0.00 | 0.03(1) | 2.4(2) | 0.00 | 0.00 | 1.9(8) | 0.04(2) | 0.05(2) |
| $P_2O_5$ | 0.89(9) | 0.00 | 0.03(1) | 0.03(1) | 0.00 | 0.00 | 0.05(3) | 0.00 | 0.00 |
| $ZrO_2$ | 0.74(5) | 0.00 | 0.28(7) | – | – | – | – | – | – |
| SrO | 0.1(1) | 0.00 | 0.00 | – | – | – | – | – | – |
| $Yb_2O_3$ | 0.63(2) | 0.02(2) | 1.04(10) | – | – | – | – | – | – |
| $La_2O_3$ | 0.65(6) | 0.00 | 0.00 | – | – | – | – | – | – |
| $Sc_2O_3$ | 0.51(1) | 0.15(1) | 1.64(9) | – | – | – | – | – | – |
| Total | 66.02(80) | 100.39(34) | 100.11(53) | 55.4(21) | 99.8(3) | 97.62(45) | 41.86(160) | 99.97(36) | 96.94(65) |

**Table 3.** (Contd.)

| Component | KTr-7 | | | KTr-8 | | KTr-10 | | | KTr-11 | |
|---|---|---|---|---|---|---|---|---|---|---|
| | *L* | *Opx* | *Grt* | *L* | *Opx* | *L* | *Opx* | *Grt* | *L* | *Opx* |
| | 23 | 10 | 9 | 14 | 12 | 11 | 4 | 4 | 25 | 3 |
| $SiO_2$ | 17.5(31) | 55.89(1) | 42.5(1) | 13.4(2) | 56.1(2) | 12.4(5) | 56.4(1) | 42.79(4) | 27.5(17) | 57.0(2) |
| $TiO_2$ | 2.0(2) | 0.19(2) | 0.7(2) | 2.45(4) | 0.27(2) | 2.1(2) | 0.23(1) | 0.52(3) | 1.32(10) | 0.09(1) |
| $Al_2O_3$ | 2.0(4) | 2.7(2) | 21.8(2) | 1.50(3) | 2.63(10) | 1.53(11) | 2.6(1) | 22.8(1) | 3.1(3) | 2.1(1) |
| $Cr_2O_3$ | 0.08(3) | 0.29(3) | 1.43(5) | 0.06(1) | 0.26(1) | 0.04(2) | 0.21(1) | 0.95(2) | 0.13(2) | 0.28(2) |
| FeO | 7.1(4) | 5.5(1) | 6.1(1) | 7.24(7) | 5.84(5) | 7.8(3) | 5.20(5) | 6.06(6) | 6.7(2) | 36.5(3) |
| MgO | 22.8(6) | 35.2(2) | 24.8(1) | 21.7(1) | 34.8(1) | 27.1(7) | 35.79(9) | 25.9(2) | 28.2(6) | 4.20(5) |
| CaO | 2.6(1) | 0.15(1) | 0.43(1) | 18.7(1) | 0.90(3) | 12.2(4) | 0.37(2) | 1.25(2) | 10.4(11) | 0.56(1) |
| $Na_2O$ | 0.5(1) | 0.05(1) | 0.00 | 0.46(4) | 0.06(1) | 0.32(9) | 0.04(2) | 0.03(1) | 0.23(4) | 0.00 |
| $K_2O$ | 1.2(4) | 0.00 | 0.00 | 1.45(6) | 0.03(2) | 1.9(2) | 0.00 | 0.00 | 1.1(2) | 0.00 |
| $P_2O_5$ | 0.03(1) | 0.00 | 0.00 | 0.95(6) | 0.00 | 0.88(8) | 0.00 | 0.02(1) | 0.53(6) | 0.00 |
| $ZrO_2$ | – | – | – | 0.04(1) | 0.00 | 0.12(3) | 0.00 | 0.06(2) | 0.06(2) | 0.00 |
| SrO | – | – | – | – | – | – | – | – | – | – |
| $Yb_2O_3$ | – | – | – | 0.00 | 0.00 | 0.02(2) | 0.00 | 0.04(1) | 0.00 | 0.00 |
| $La_2O_3$ | – | – | – | 0.03(2) | 0.00 | 0.08(3) | 0.00 | 0.00 | 0.05(2) | – |
| $Sc_2O_3$ | – | – | – | – | – | 0.00 | – | 0.06(1) | 0.00 | – |
| Total | 55.81(332) | 99.88(27) | 97.76(25) | 67.98(14) | 100.89(18) | 66.49(113) | 100.84(11) | 100.48(32) | 79.32(131) | 100.73(30) |

| Component | KTr-12 | | | | KTr-13 | | | | KTr-15 | | | |
|---|---|---|---|---|---|---|---|---|---|---|---|---|
| | *L* | *Grt* | *Opx* | *Cpx* | *L* | *Opx* | *Grt* | *Cpx* | *L* | *Opx* | *Grt* | *Cpx* |
| | 16 | 9 | | 18 | 18 | 14 | 2 | 12 | 20 | 10 | 3 | 17 |
| $SiO_2$ | 13.6(11) | 42.2(3) | 56.2(3) | 54.6(2) | 13.5(8) | 55.7(1) | 42.17 | 53.9(4) | 9.0(7) | 56.1(5) | 42.0(1) | 54.5(4) |
| $TiO_2$ | 1.67(8) | 0.57(7) | 0.15(1) | 0.19(1) | 1.69(5) | 0.20(2) | 0.56 | 0.26(2) | 1.85(11) | 0.18(1) | 0.59(4) | 0.24(2) |
| $Al_2O_3$ | 1.4(1) | 21.9(4) | 2.04(4) | 2.28(6) | 1.54(10) | 2.76(10) | 22.20 | 2.8(2) | 0.88(8) | 1.79(4) | 21.98(6) | 2.1(3) |
| $Cr_2O_3$ | 0.04(1) | 1.04(3) | 0.17(1) | 0.22(2) | 0.03(1) | 0.23(2) | 1.20 | 0.28(3) | 0.02(1) | 0.14(2) | 0.99(5) | 0.20(2) |
| FeO | 6.06(12) | 6.87(6) | 6.16(8) | 4.52(6) | 6.3(2) | 6.05(6) | 6.75 | 4.17(11) | 5.8(2) | 6.82(5) | 7.73(3) | 4.6(1) |
| MgO | 16.5(2) | 21.9(2) | 33.4(1) | 22.6(2) | 16.3(2) | 33.5(1) | 21.57 | 21.8(5) | 15.6(2) | 33.2(5) | 21.1(8) | 21.8(11) |
| CaO | 24.6(5) | 5.4(1) | 2.25(11) | 15.0(2) | 25.4(3) | 2.03(8) | 5.66 | 16.4(9) | 26.7(4) | 2.0(3) | 5.38(7) | 16.1(9) |
| $Na_2O$ | 0.27(3) | 0.03(1) | 0.06(1) | 0.25(2) | 0.25(3) | 0.04(1) | 0.00 | 0.18(2) | 0.27(2) | 0.08(2) | 0.06(4) | 0.31(3) |
| $K_2O$ | 1.12(10) | 0.04(2) | 0.04(2) | 0.05(2) | 1.41(6) | 0.00 | 0.00 | 0.00 | 1.5(1) | 0.06(3) | 0.00 | 0.10(5) |
| $P_2O_5$ | 0.65(8) | 0.04(4) | 0.00 | 0.00 | 0.71(4) | 0.00 | 0.00 | 0.00 | 0.74(5) | 0.00 | 0.00 | 0.00 |
| $ZrO_2$ | 0.09(2) | 0.04(2) | 0.00 | 0.00 | 0.09(2) | 0.00 | 0.04 | 0.00 | 0.09(2) | 0.00 | 0.03(1) | 0.00 |
| SrO | – | – | – | – | – | – | – | – | – | – | – | – |
| $Yb_2O_3$ | 0.00 | 0.04(2) | 0.00 | 0.00 | 0.03(2) | 0.00 | 0.07 | 0.00 | 0.00 | 0.00 | 0.04(2) | 0.00 |
| $La_2O_3$ | 0.06(2) | 0.00 | 0.00 | 0.00 | 0.06(2) | 0.00 | 0.00 | 0.00 | 0.07(1) | 0.00 | 0.00 | 0.00 |
| $Sc_2O_3$ | 0.00 | 0.05(1) | 0.00 | 0.00 | 0.02(1) | 0.00 | 0.06 | 0.00 | 0.02(1) | 0.00 | 0.05(1) | 0.00 |
| Total | 66.07(107) | 100.12(48) | 100.47(28) | 99.71(23) | 67.33(98) | 100.51(29) | 100.28 | 99.79(32) | 62.54(100) | 100.37(67) | 99.95(27) | 99.95(59) |

Note: Numbers in parentheses show one standard deviation in terms of the last significant digit. Dashes indicate component not analyzed.
* Here and in Table 4, run number.
** Here and in Table 4, phase.
*** Number of analyses.

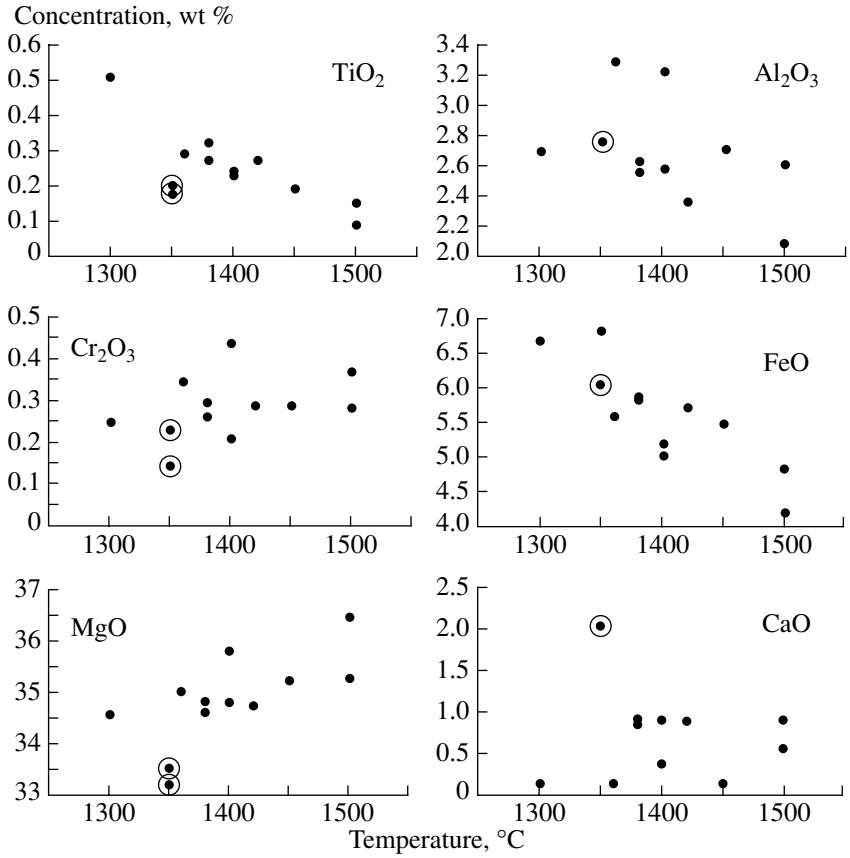


**Fig. 2.** Compositions of experimental orthopyroxene as a function of temperature. The encircled points correspond to the compositions of orthopyroxene coexisting with clinopyroxene.

behavior of CaO. In experiments with low initial Ca content, the concentration of CaO is low and almost invariant with temperature. In the experiments with initial mixes containing about 10 wt % CaO, it is accumulated in residual melts up to 20–25 wt % CaO at 1350–1400°C. Clinopyroxene-saturated melts contain about 25 wt % CaO. The concentrations of incompatible minor elements (Ti, P, and K) increase with decreasing temperature, and the considerable scatter in their contents is due to the compositional differences between the starting materials.

### *Comparison of Results Obtained by Electron Microprobe Analysis and LA-ICP-MS*

The major-element compositions of quench aggregates formed from carbonate–silicate melts are commonly analyzed with an electron microprobe using a defocused beam with a diameter of 20–50 μm. The concentrations of trace elements in such aggregates were determined using an ion microprobe (Blundy and Dalton, 2000), a proton microprobe (Sweeney et al., 1992, 1995), and LA-ICP-MS (Adam and Green, 2001; Klemme et al., 1995; Keshav et al., 2005). Klemme and Dalpe (2003) established a good consistency between the compositions of carbonate melts obtained by ion microprobe analysis and LA-ICP-MS. However, such data are still very limited. Since the procedure of LA-ICP-MS analysis includes the evaporation of sample material under the influence of a laser beam, element fractionation is possible at the expense of the nonuniform evaporation of quench crystals. To check this possibility, we performed experiments with mix KCa3T05 containing 0.5 wt % of $Sc_2O_3$, $ZrO_2$, $Nb_2O_5$, $La_2O_3$, and $Yb_2O_3$, The concentrations of these elements (as well as Sr, which is also high in the starting kimberlite composition) in the quenched melts from these experiments were high enough for reliable electron microprobe analysis. Figures 5 and 6 compare the results obtained by the two methods for quenched melts and orthopyroxene. The results of analysis for $SiO_2$, La, Sr, and Yb in the quench aggregates (Fig. 5) appeared to be in good agreement; the discrepancy is nonsystematic and usually lower than 10%. Approximately the same deviations were obtained for the analyses of minor elements in orthopyroxene (Fig. 6). It should be taken into account that the heterogeneity of experimental phases also contributed to the observed scatter, and we conclude therefore that the data presented in Figs. 5 and 6 indicate the plausibility of the results obtained by LA-ICP-MS for trace elements (at least for La, Sr, and Yb). The concentrations of Zr and Sc determined by LA-

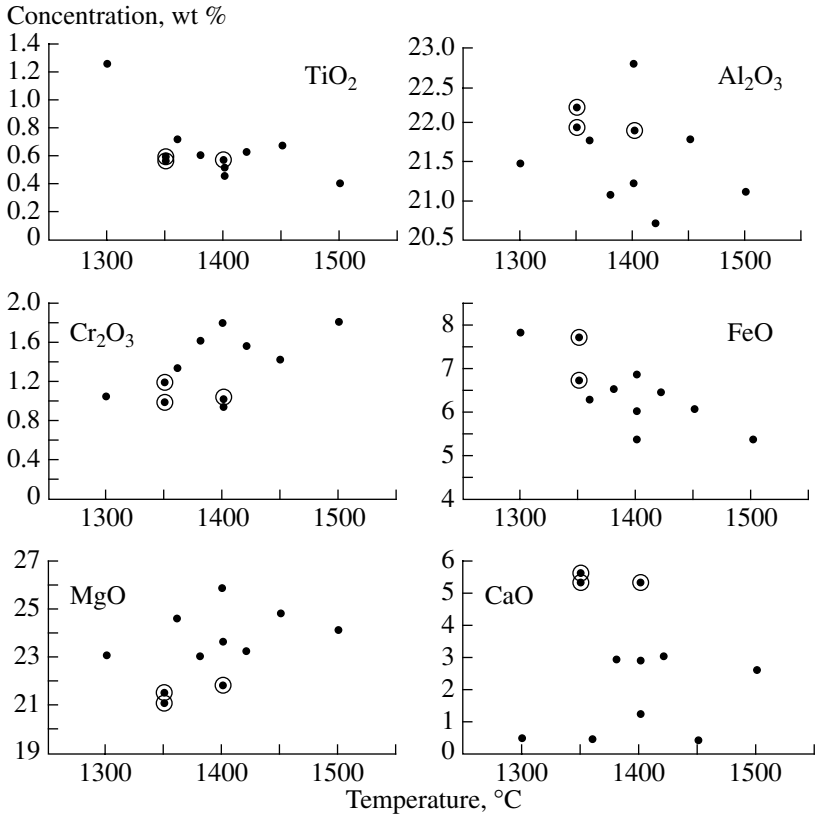


**Fig. 3.** Compositions of experimental garnet as a function of temperature. The encircled points correspond to the compositions of garnet coexisting with clinopyroxene.

ICP-MS are systematically higher than the values obtained by electron microprobe analysis (Fig. 5). However, the discrepancies between the two methods were about 10%, and we did not attempt to introduce corrections to the measured concentrations of these elements in quenched melts. The results suggest that the concentrations of trace elements in the experimental melts were determined with an accuracy of about 10%.

### *Partitioning of Trace Elements*

The concentrations of trace elements determined by LA-ICP-MS are given in Table 4, and the mineral–melt partition coefficients ($D_i^{\text{mineral}/L}$ = mass concentration in mineral/mass concentration in melt) are shown in Table 5. For most elements, the data obtained in our experiments did not reveal any regular variations in partition coefficients depending on the concentration of CaO in melt. In order to quantify changes in element behavior associating with the transition from carbonate-dominated (low-temperature) to carbonate–silicate (high-temperature) compositions, the melts were arbitrarily divided into two parts, carbonate and kimberlite, at a level of 12–15 wt % $SiO_2$. Median values of partition coefficients were determined for each of these groups (Table 5). The difference between the carbonate and kimberlite melts was negligible for the partitioning of most elements. In such cases, median values were calculated for the complete data set. Significant differences between the carbonate and kimberlite melts were observed only for the orthopyroxene–melt partition of compatible and moderately incompatible elements (Sc, V, Cr, and Co). For all other elements, the experimental and analytical errors appeared to be more significant than the possible effect of composition or temperature. The garnet–melt partition coefficients of trace elements were determined mainly for the kimberlite melts. At low temperatures, garnet crystals were too small for reliable trace-element analysis by LA-ICP-MS. Thus, only electron microprobe data are available for garnet–carbonate melt partitioning (Table 5).

The analyses of the most incompatible elements (Ba, Nb, Ta, and La) in orthopyroxene show considerable scatter. This is related to the very low contents of these elements in the mineral structure and the strong influence of contamination by even a small amount of quenched melt (for instance, in inclusions) during analysis. Because of this, the $D^{Opx/L}$ values of these elements are not given in Table 5. Among other elements, the lowest $D^{Opx/L}$ values were obtained for light REE (<0.01). Heavy REE, Y, Zr, Hf, and Sr show $D^{Opx/L}$ of 0.01–0.1. Higher values (but significantly lower than 1) were determined for Li, Ti, Sc, V, and Zn. Co occurs in

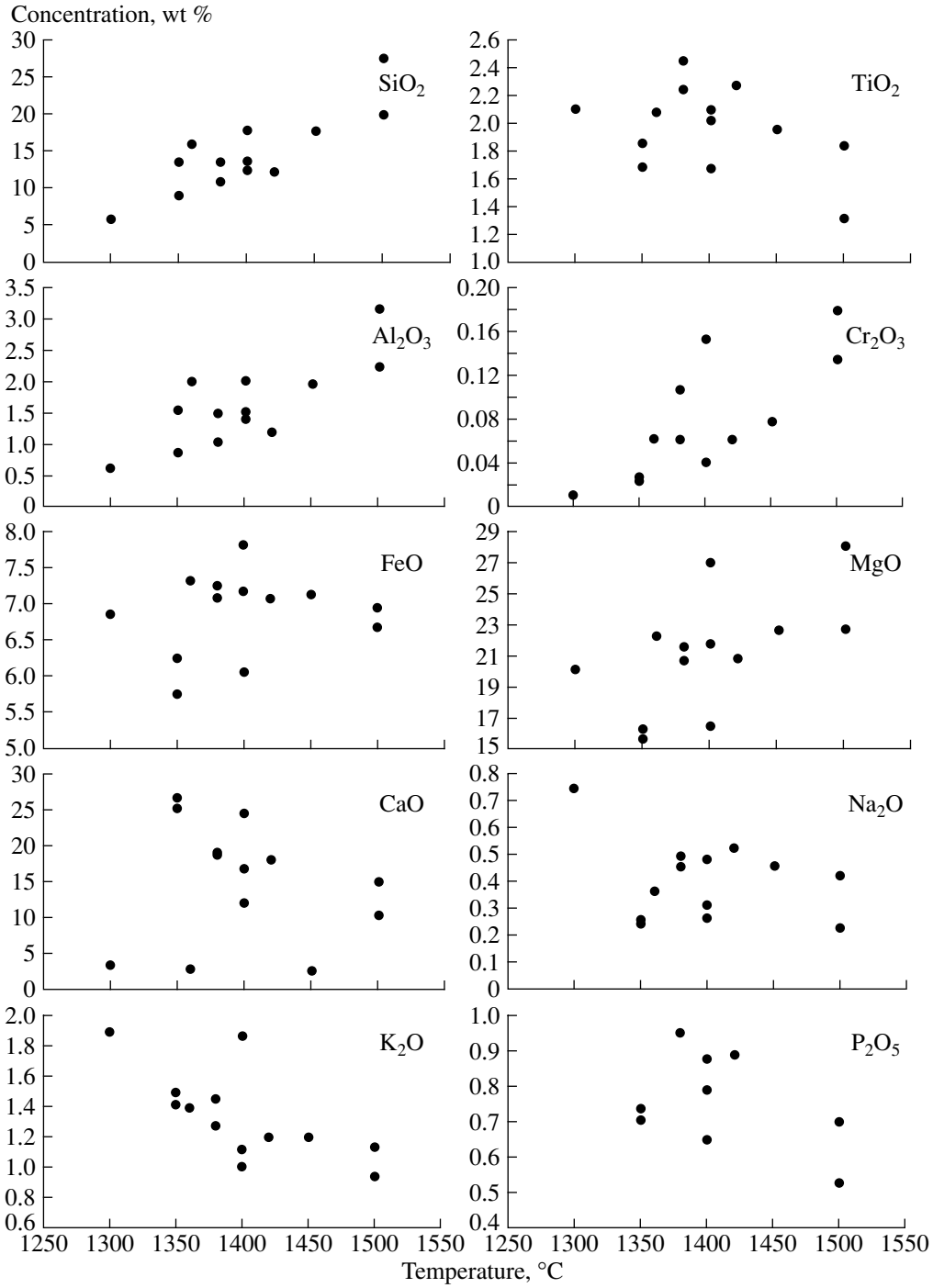


**Fig. 4.** Concentrations of major elements in quenched melts as a function of experimental temperature.

approximately equal amounts in orthopyroxene and melt. Only Cr is distinctly compatible in orthopyroxene ($D^{Opx/L} > 1$). Significant differences between the $D^{Opx/L}$ values of carbonate and kimberlite melts were observed only for moderately incompatible (Sc and V) and compatible (Cr) elements. The $D^{Opx/L}$ values of these elements are significantly higher for carbonate melts compared with kimberlite melts (Table 5).

The garnet–melt partitioning data show the same characteristics as orthopyroxene–melt partitioning, but the $D^{Grt/L}$ values are somewhat higher than $D^{Opx/L}$. For the most incompatible elements (La, Nb, and Ba), $D^{Grt/L}$ is from 0.03 to 0.04, and a number of elements show $D^{Grt/L} > 1$ (heavy REE, Sc, V, and Cr). The $D^{Grt/L}$ values for Sc and Cr are significantly higher for carbonate melts.

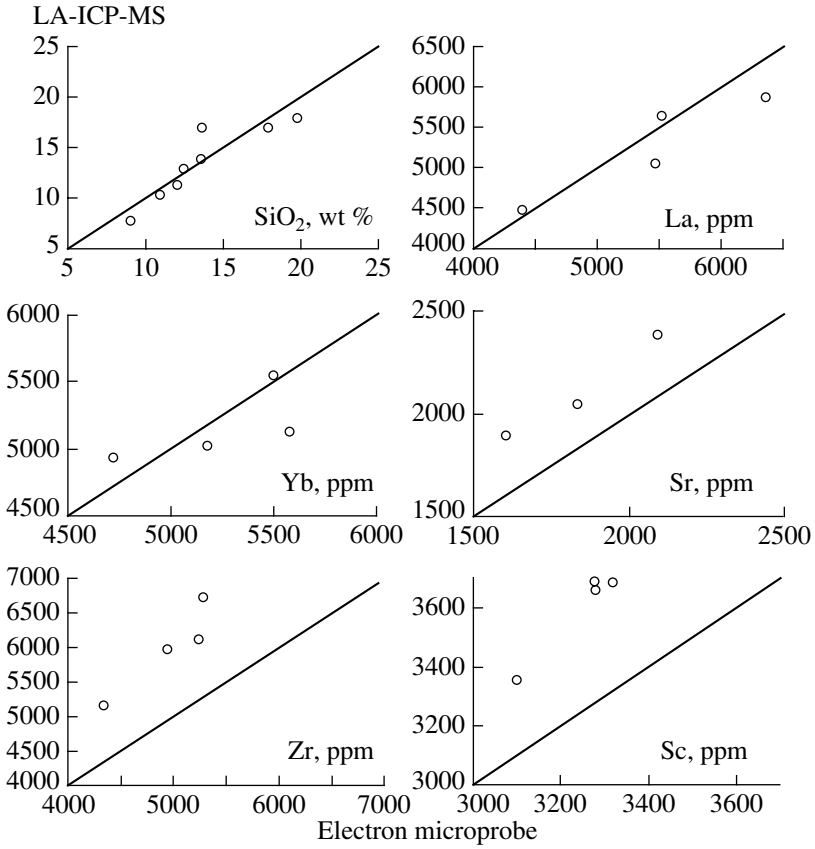


**Fig. 5.** Comparison of the concentrations of $SiO_2$ and minor elements in quenched melts determined by electron microprobe analysis (defocused beam, average of 20–40 measurements) and LA-ICP-MS.

The clinopyroxene–melt partitioning of elements was estimated for carbonate melts only on the basis of electron microprobe analyses (Table 5). In general, the $D^{Cpx/L}$ values for moderately incompatible (Ti, Sc, and Zn) and compatible (V, Cr, and Co) elements are higher than $D^{Opx/L}$ but lower than $D^{Grt/L}$ (Table 5).

## DISCUSSION

### *Comparison with Published Data*

Up to now, the partitioning of trace elements between orthopyroxene and carbonate and carbonate–silicate melts was not systematically studied at high pressures. There are several determinations of the composition of orthopyroxene in equilibrium with carbonatite melts at pressures of 2.0–4.6 GPa and 1000–1300°C (Wallace and Green, 1988; Dalton and Wood, 1993; Sweeney et al., 1995; Yaxley and Green, 1996), including some minor and trace elements (Ti, Cr, Zr, Y, Lu, and Sr). These data are compared with our results in Fig. 7. Our estimates coincide with the results of other authors for Cr and Zn. The $D_{Ti}^{Opx/L}$ value obtained from our experiments (0.1) is significantly lower than in most other studies (about 1) but is almost identical to the value reported by Sweeney et al. (1995). The $D^{Opx/L}$ values reported by these authors for Sr, Zr, and Y are somewhat higher than our estimates, but the differences are no higher than the experimental uncertainties. A more significant discrepancy was obtained for $D_{Lu}^{Opx/L}$: 0.022 according to our results and 0.5 after Sweeney et al. (1995). This difference can be related to the higher temperatures of our experiments: Sweeney et al. (1995) reported the results of a single experiment at 4.6 GPa and 1250°C. This suggestion is supported by a slight increase in the partition coefficients of Cr, V, and Sc accompanying the transition from kimberlite to carbonatite compositions, which indicates a possible temperature effect on the partitioning of compatible and moderately incompatible elements.

The published data on the partitioning of trace elements between garnet and carbonate–silicate melts are more representative, although also scanty (Adam and Green, 2001; Sweeney, 1994; Sweeney et al., 1992, 1995). These results were obtained at pressures of 2.5–4.6 GPa and relatively low temperatures (1000–1200°C). A comparison with our data is shown in Fig. 8. The following characteristics can be pointed out: low $D^{Grt/L}$ values for Ta, Nb, and Sr; moderately incompatible behavior of Zr, Hf, Ti, and Y; and compatibility of heavy REE, Sc, and Cr in garnet. Our results are in

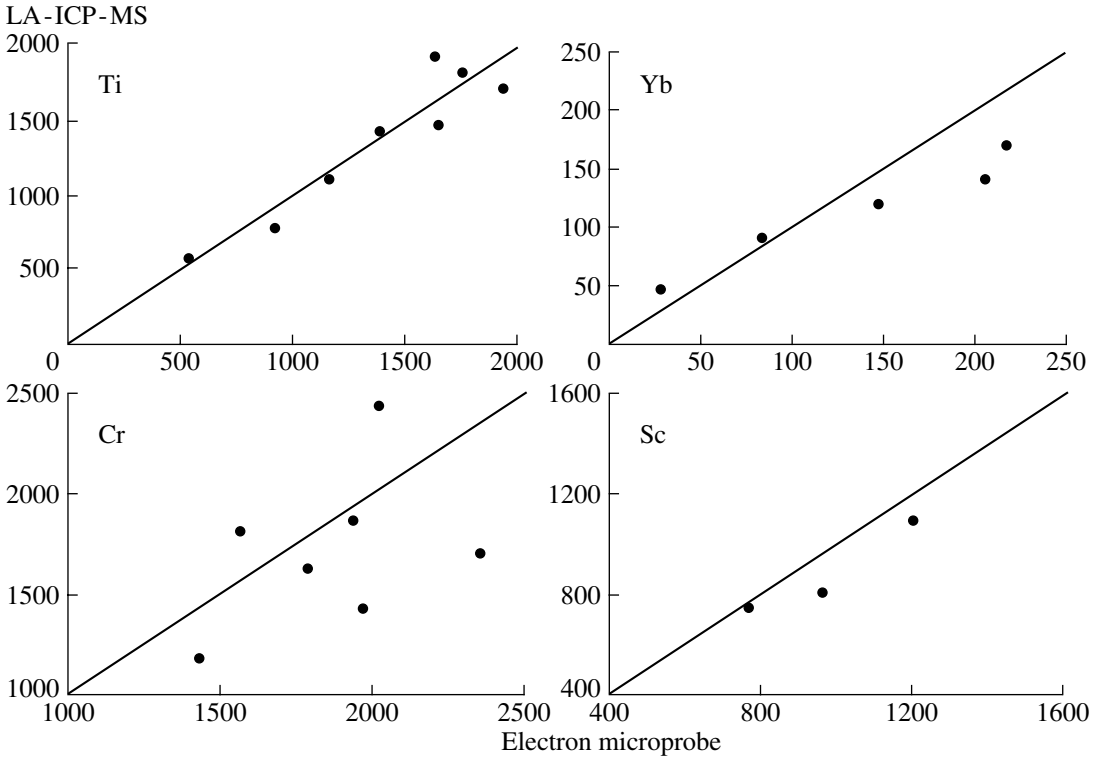


**Fig. 6.** Comparison of the concentrations of minor elements in orthopyroxene (ppm) determined by electron microprobe analysis (average of 10–15 measurements) and LA-ICP-MS.

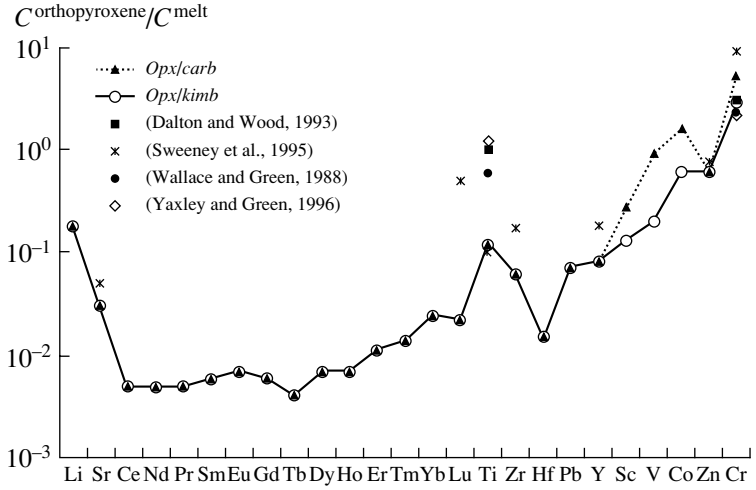


**Fig. 7.** Trace element partition coefficients between orthopyroxene and carbonate and kimberlite melt. Our results are shown by solid (kimberlite melts with >15 wt % $SiO_2$) and dashed (carbonate melts with <15 wt % $SiO_2$) lines. The partition coefficients of most elements are identical for the carbonate and kimberlite melts. Symbols show the available literature data on element partitioning between orthopyroxene and carbonate melt at pressures of 2.0–4.6 GPa and temperatures of 1000–1300°C.

good agreement with the data of Sweeney (1994) and Sweeney et al. (1992, 1995) for the most incompatible elements (Ba, Sr, Nb, Ta, and Ce). Our $D^{Grt/L}$ values for compatible and moderately incompatible elements (heavy REE, Ti, Zr, Y, and Cr) are systematically lower than the data of these authors. Adam and Green (2001) obtained more considerable differences between the incompatible and compatible elements. The partition coefficients of the most incompatible elements (Sr, Ba, Nb, and La) obtained by these authors are approximately an order of magnitude lower than our estimates, whereas the $D^{Grt/L}$ values for moderately incompatible

**Table 4.** Concentrations of trace elements (ppm) in experimental phases analyzed by LA-ICP-MS

| Component | KTr-1 | | | KTr-2 | | | KTr-3 | | |
|---|---|---|---|---|---|---|---|---|---|
| | *L* | *Opx* | *Grt* | *L* | *Opx* | *Grt* | *L* | *Opx* | *Grt* |
| Li | – | – | – | – | – | – | – | – | – |
| Sc | 3661(71) | 747(58) | 6126(217) | 3689(67) | 464(20) | 5362(43) | 3358(111) | 1097(134) | 8760(305) |
| V | – | – | 11(1) | – | 0 | 16(1) | – | – | 18(1) |
| Cr | 832(14) | 4902(150) | 9838(320) | 701(28) | 5618(220) | 8090(45) | 367(10) | 2437(102) | 5849(187) |
| Co | – | – | – | – | – | – | – | – | – |
| Zn | – | – | – | – | – | – | – | – | – |
| Rb | – | – | – | – | – | – | – | – | – |
| Sr | 1899(42) | – | 165(3) | 2048(68) | – | 71(8) | 2391(54) | 0 | 61(3) |
| Y | – | – | – | – | – | – | – | – | – |
| Zr | 5973(103) | 21(11) | 1280(45) | 6111(151) | 6(0.6) | 1014(17) | 5164(182) | 33(12) | 1136(39) |
| Nb | 3966(118) | – | 310(6) | 4171(98) | – | 102(15) | 4715(160) | – | 100(4) |
| Ba | 1917(71) | – | 143(3) | 2122(44) | – | 78(7) | 2377(38) | – | 91(4) |
| La | 4480(159) | – | 174(6) | 5055(214) | – | 168(17) | 5869(170) | – | 183(6) |
| Ce | – | – | – | – | – | – | – | – | – |
| Pr | – | – | – | – | – | – | – | – | – |
| Nd | – | – | – | – | – | – | – | – | – |
| Sm | – | – | – | – | – | – | – | – | – |
| Eu | – | – | – | – | – | – | – | – | – |
| Gd | – | – | – | – | – | – | – | – | – |
| Tb | – | – | – | – | – | – | – | – | – |
| Dy | – | – | – | – | – | – | – | – | – |
| Ho | – | – | – | – | – | – | – | – | – |
| Er | – | – | – | – | – | – | – | – | – |
| Tm | – | – | – | – | – | – | – | – | – |
| Yb | 4940(245) | 120(15) | 7055(233) | 5034(190) | 33(2) | 6366(37) | 5141(215) | 170(63) | 7427(239) |
| Lu | – | – | – | – | – | – | – | – | – |
| Hf | – | – | – | – | – | – | – | – | – |
| Ta | – | – | – | – | – | – | – | – | – |
| Pb | – | – | – | – | – | – | – | – | – |

**Table 4.** (Contd.)

| Component | KTr-4 | | KTr-5 | | KTr-7 | | KTr-8 | |
|---|---|---|---|---|---|---|---|---|
| | *L* | *Opx* | *L* | *Grt* | *L* | *Opx* | *L* | *Opx* |
| Li | – | – | 128(4) | 15(1) | 92(9) | 27(3) | 480(113) | 23(4) |
| Sc | 3687(29) | 807(18) | 60(9) | 158(1) | 55(3) | 14(1.6) | 288(102) | 12(3) |
| V | – | – | 172(7) | 231(2) | 170(10) | 110(5) | 515(79) | 93(9) |
| Cr | 424(10) | – | 616(24) | 3166(18) | 740(31) | 1427(124) | 632(16) | 1627(67) |
| Co | – | – | 97(3) | 82(1) | 82(4) | 107(7) | 373(90) | 102(14) |
| Zn | – | – | 163(4) | 47(1) | 140(11) | 89(10) | 491(76) | 83(14) |
| Rb | – | – | 134(5) | 0 | 116(12) | 14.7(6) | 464(86) | 0 |
| Sr | 2302(65) | – | 2305(69) | 126(1) | 1830(218) | 6(2) | 951(57) | 0 |
| Y | – | – | 179(6) | 93(1) | 148(13) | 2.1(0.3) | 532(86) | 1.6(0.3) |
| Zr | 6728(400) | 39(11) | 627(32) | 193(2) | 535(55) | 3.4(0.4) | 759(15) | 3.7(0.4) |
| Nb | 4981(273) | – | 375(16) | 31(1) | 305(37) | 0 | 717(46) | 0 |
| Ba | 2251(83) | – | 3029(168) | 175(1) | 2180(145) | 5.1(3) | 909(74) | 5.9(1) |
| La | 5645(322) | 5.4(1.2) | 315(15) | 18(1) | 243(122) | 0 | 621(36) | 0 |
| Ce | – | – | 482(24) | 35(1) | 373(36) | 1.9(1) | 689(20) | 0 |
| Pr | – | – | 180(8) | 12(1) | 138(17) | 0.6(0.4) | 542(85) | 0 |
| Nd | – | – | 198(11) | 14(1) | 147(19) | 0.7(0.3) | 533(77) | 1.6(0.4) |
| Sm | – | – | 127(8) | 11(1) | 94(9) | 0.6(0.2) | 448(93) | 0 |
| Eu | – | – | 110(7) | 12(1) | 80(9) | 0.6(0.3) | 415(88) | 0 |
| Gd | – | – | 113(6) | 17(1) | 88(9) | 0.7(0.3) | 417(98) | 0 |
| Tb | – | – | 115(6) | 26(1) | 88(8) | 0.8(0.2) | 408(93) | 0.7(0.2) |
| Dy | – | – | 103(6) | 34(1) | 78(7) | 1(0.2) | 400(96) | 0.9(0.3) |
| Ho | – | – | 73(6) | 38(1) | 54(6) | 1(0.2) | 329(108) | 0.8(0.2) |
| Er | – | – | 103(8) | 80(1) | 78(7) | 1.7(0.4) | 390(101) | 1.5(0.2) |
| Tm | – | – | 112(8) | 114(1) | 83(8) | 2.1(0.2) | 405(100) | 1.8(0.3) |
| Yb | 5548(230) | 141(25) | 111(7) | 144(1) | 79(7) | 2.4(0.4) | 395(110) | 2.1(0.3) |
| Lu | – | – | 106(7) | 180(1) | 78(7) | 3.1(0.5) | 375(107) | 2.5(0.5) |
| Hf | – | – | 328(22) | 118(1) | 240(22) | 3.7(0.4) | 611(56) | 5.2(2) |
| Ta | – | – | 254(16) | 19(1) | 179(19) | 0 | 599(77) | 0 |
| Pb | – | – | 208(24) | 69(1) | 173(40) | 47(14) | 505(63) | 5.5(2) |

**Table 4.** (Contd.)

| Component | KTr-10 | | KTr-11 | | KTr-13 | | | KTr-15 | |
|---|---|---|---|---|---|---|---|---|---|
| | *L* | *Opx* | *L* | *Opx* | *L* | *Opx* | *Grt* | *L* | *Opx* |
| Li | 155(11) | 27(7) | 246(31) | 26(4) | 167(13) | 51(8) | 8(3) | 157(11) | 65(10) |
| Sc | 118(20) | 20(1.5) | 176(21) | 15(1.5) | 86(5) | 99(31) | 410(14) | 74(6) | 58(14) |
| V | 300(42) | 201(17) | 561(43) | 121(12) | 303(31) | 305(77) | 702(23) | 230(7) | 287(51) |
| Cr | 223(27) | 1182(84) | 1325(15) | 1865(71) | 358(47) | 1817(94) | 3420(105) | 299(17) | 1430(54) |
| Co | 180(27) | 189(7) | 313(35) | 174(8) | 156(11) | 223(7) | 185(6) | 117(5) | 252(10) |
| Zn | 216(24) | 156(19) | 473(63) | 127(13) | 274(19) | 195(22) | 84(6) | 190(14) | 235(37) |
| Rb | 184(19) | 0 | 232(26) | 3.8(2) | 183(13) | 20(7) | 0 | 174(8) | 10(3) |
| Sr | – | – | – | – | – | – | – | – | – |
| Y | 317(30) | 2.8(0.3) | 403(38) | 2.8(0.8) | 302(15) | 85(12) | 282(10) | 278(14) | 44(3) |
| Zr | 644(23) | 6(0.6) | 940(36) | 3.5(0.9) | 1033(30) | 174(25) | 367(13) | 1044(28) | 110(17) |
| Nb | 512(44) | 0 | 683(44) | 0 | 642(30) | 73(16) | 8(1) | 593(20) | 30(9) |
| Ba | – | – | – | – | – | – | – | – | – |
| La | 427(38) | 0 | 558(36) | 0 | 545(27) | 54(19) | 0 | 498(19) | 36(16) |
| Ce | 502(34) | 0 | 784(36) | 2.2(1.3) | 803(20) | 101(34) | 0 | 745(26) | 46(20) |
| Pr | 310(31) | 0 | 375(34) | 0.7(0.3) | 322(21) | 34(13) | 0 | 277(10) | 15(2) |
| Nd | 314(31) | 0 | 380(34) | 7(4) | 329(19) | 36(13) | 6(1) | 286(13) | 16(4) |
| Sm | 228(27) | 0 | 262(28) | 0.7(0.5) | 210(14) | 25(25) | 13(1) | 184(9) | 11(2) |
| Eu | 203(25) | 0 | 232(26) | 0.7(0.5) | 181(14) | 23(9) | 19(1) | 157(8) | 10(4) |
| Gd | 214(28) | 0.7(0.1) | 240(27) | 1(0.6) | 187(12) | 27(12) | 38(2) | 172(11) | 12(3) |
| Tb | 212(25) | 0.9(0.1) | 244(25) | 1(0.5) | 185(11) | 32(13) | 68(3) | 168(11) | 14(4) |
| Dy | 201(29) | 1.3(0.2) | 224(24) | 1.3(0.5) | 168(13) | 36(16) | 97(4) | 151(10) | 19(6) |
| Ho | 148(21) | 1.1(0.1) | 167(19) | 1.1(0.3) | 116(9) | 32(16) | 111(4) | 103(7) | 15(5) |
| Er | 194(27) | 2.2(0.2) | 231(23) | 2.1(0.4) | 161(13) | 59(18) | 236(8) | 144(10) | 32(3) |
| Tm | 202(29) | 2.7(0.3) | 247(29) | 2.5(0.5) | 168(14) | 80(26) | 329(11) | 149(11) | 41(4) |
| Yb | 185(27) | 3.2(0.2) | 235(27) | 3(0.5) | 150(12) | 91(18) | 415(14) | 131(10) | 47(7) |
| Lu | 185(26) | 4(0.2) | 239(27) | 3.5(0.3) | 145(11) | 109(24) | 523(17) | 127(10) | 57(10) |
| Hf | 443(46) | 7.3(0.8) | 580(39) | 3.4(1.5) | 490(32) | 98(16) | 211(7) | 469(29) | 68(12) |
| Ta | 396(60) | 0.9(0.6) | 453(39) | 0 | 397(28) | 47(17) | 8(1) | 362(24) | 29(14) |
| Pb | 191(29) | 14(9) | 291(27) | 2.2(0.8) | 216(14) | 25(8) | 10(1) | 193(16) | 16(5) |

**Table 5.** Partition coefficients of trace elements between minerals and carbonate ($SiO_2$ < 13 wt %) and kimberlite ($SiO_2$ > 13 wt %) melts

| Element | *Opx/L* | | *Grt/L* | | *Cpx/L* |
|---|---|---|---|---|---|
| | kimberlite melt | carbonate melt | kimberlite melt | carbonate melt | carbonate melt |
| Li | 0.18 | 0.18 | 0.08 | – | – |
| Sc | 0.13 | 0.27 | 1.7 | 2.6 | 0.6 |
| Ti | 0.12 | 0.12 | 0.32 | 0.32 | 0.13 |
| V | 0.2 | 0.9 | 1.8 | – | 1.4 |
| Cr | 2.9 | 5.2 | 15 | 25 | 6.6 |
| Co | 0.6 | 1.6 | 1 | – | 1.3 |
| Zn | 0.6 | 0.6 | 0.3 | – | 0.7 |
| Sr | 0.03 | 0.03 | 0.03 | 0.03 | – |
| Y | 0.08 | 0.08 | 0.7 | – | – |
| Zr | 0.06 | 0.06 | 0.2 | 0.2 | – |
| Nb | – | – | 0.02 | 0.02 | – |
| Ba | – | – | 0.04 | 0.04 | – |
| La | – | – | 0.07 | – | – |
| Ce | 0.005 | 0.005 | 0.07 | – | – |
| Pr | 0.005 | 0.005 | 0.05 | – | – |
| Nd | 0.005 | 0.005 | 0.07 | – | – |
| Sm | 0.006 | 0.006 | 0.07 | – | – |
| Eu | 0.007 | 0.007 | 0.11 | – | – |
| Gd | 0.006 | 0.006 | 0.18 | – | – |
| Tb | 0.004 | 0.004 | 0.29 | – | – |
| Dy | 0.007 | 0.007 | 0.45 | – | – |
| Ho | 0.007 | 0.007 | 0.74 | – | – |
| Er | 0.011 | 0.011 | 1.1 | – | – |
| Tm | 0.014 | 0.014 | 1.5 | – | – |
| Yb | 0.024 | 0.024 | 1.5 | 1.4 | – |
| Lu | 0.022 | 0.022 | 2.6 | – | – |
| Hf | 0.015 | 0.015 | 0.4 | – | – |
| Ta | – | – | 0.05 | – | – |
| Pb | 0.07 | 0.07 | 0.3 | – | – |

and compatible elements are slightly higher (Fig. 8) and approach the data of Sweeney (1994) and Sweeney et al. (1992, 1995).

The observed differences between our and published estimates are not fundamental (Fig. 8). The similarity of $D^{Grt/L}$ patterns in Fig. 8 suggests that the discrepancies are probably not related to some errors in experimental and analytical methods and probably reflect the difference in the behavior of elements under different experimental conditions. Similar to the orthopyroxene–melt partitioning, the most important factor is probably the relatively high temperature of our experiments.

### *Indicators of Mantle Metasomatism Caused by Carbonate and Silicate Melts*

The relative enrichment of mantle magma sources in the most incompatible elements is explained by the migration of small portions of near-solidus mantle melts, including carbonate ones (Yaxley et al., 1991; Rudnick et al., 1993). It is supposed that the character of the agent of mantle metasomatism (silicate melt, carbonate melt, or fluid) can be recognized on the basis of geochemical indicators. In particular, high contents of Sr, Ba, and light REE coupled with low contents of high field strength elements (Ti, Nb, Ta, Hf, and Zr) were proposed as characteristic signatures of carbonate

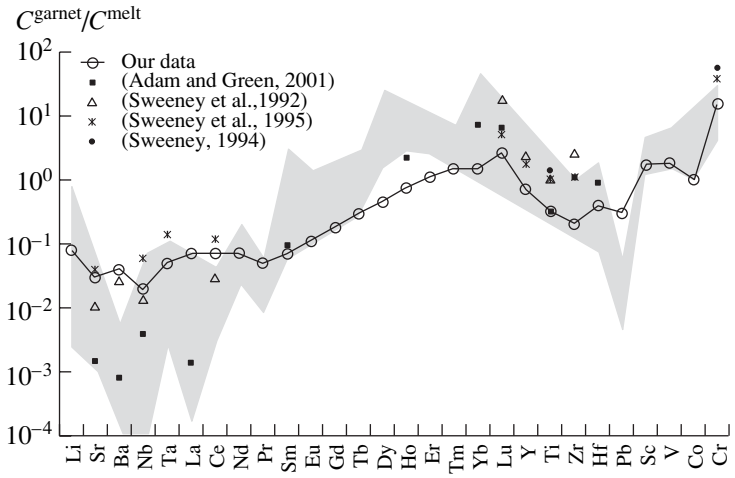


**Fig. 8.** Trace element partition coefficients between garnet and melt. Our data for $CO_2$-saturated kimberlite melts are connected by the solid line. Symbols show experimental data from the literature on trace element partitioning between garnet and carbonate melt at pressures of 2.5–4.6 GPa and temperatures of 1000–1200°C. The shaded field indicates the interval of published trace element partition coefficients between garnet and $CO_2$-poor silicate melts of various compositions (Barth et al., 2002; Bennett et al., 2004; Draper et al., 2003; Green et al., 2000; Nicholls and Harris, 1980; Van Westrenen et al., 1999, 2000).

metasomatism (Yaxley et al., 1991; Ionov et al., 1993; Rudnick et al., 1993). However, there is evidence that similar geochemical parameters can be obtained by the movement of alkaline silicate melts in the mantle (Vannucci et al., 1998).

The solution of the problem of geochemical indicators of the nature of mantle metasomatic agents requires the knowledge of trace-element partition coefficients as functions of conditions and melt composition. Hence, it is interesting to compare the data obtained in our study for carbonate and carbonate–silicate ($CO_2$-bearing) melts with results for silicate melts under similar *P–T* conditions. To this end, we used data from the literature on trace element partitioning between garnet and silicate melts at 2–7 GPa (Barth et al., 2002; Bennett et al., 2004; Draper et al., 2003; Green et al., 2000; Nicholls and Harris, 1980; Van Westrenen et al., 1999, 2000). The choice of garnet was dictated by the fact that high-pressure data for this mineral are more representative than those for orthopyroxene; furthermore, the partitioning of elements between garnet and melt is more contrasting than between orthopyroxene and melt.

Figure 8 shows that the partition coefficients of the majority of elements between garnet and $CO_2$-bearing melt fall within the range reported for garnet–silicate melt partitioning. However, the slope of the spectrum is much less steep than that for silicate systems. The comparison is complicated by the sensitivity of partition coefficients to experimental conditions and melt composition. A close inspection of the available data suggests that the behavior of strongly incompatible and moderately incompatible and compatible elements is significantly different (Fig. 9). Strongly incompatible elements (Nb, Sr, light REE, etc.), Sc, Zr, and Hf are characterized by either a negligible or a weak positive correlation between $D^{Grt/L}$ and temperature. Moderately incompatible elements exhibit a distinct negative correlation with temperature, which is also supported by our results (Fig. 9). It is clearly seen that the $D^{Grt/L}$ values of some element (Dy and Gd) for the system garnet–$CO_2$-bearing melt fall on the trend formed by the data for the garnet–silicate melt system, whereas the $D^{Grt/L}$ values of Yb and Y for $CO_2$-bearing melts are significantly lower than those for silicate melts under the same temperature.

This difference is illustrated by the diagram of $D^{S/C} = D^{Grt/Carb} : D^{Grt/Sil}$, where $D^{Grt/Carb}$ and $D^{Grt/Sil}$ are the partition coefficients of elements between garnet and $CO_2$-bearing and $CO_2$-free silicate melts, respectively, at 1300–1450°C (Fig. 10). The elements showing $D^{S/C} > 1$ are more efficiently extracted by silicate melts, whereas those with $D^{S/C} < 1$, by $CO_2$-bearing (kimberlite) melt. The observed considerable differences between the $D^{S/C}$ values of neighboring elements (e.g., REE) are probably due to analytical and experimental errors. On the other hand, the general character of $D^{S/C}$ variations is rather robust and is probably related to the different properties of silicate and $CO_2$-rich melts. High $D^{S/C}$ values were obtained for Sr, Ba, Nb, Ta, and light REE. There is a gradual decrease in $D^{S/C}$ from light to heavy REE. Yttrium is similar in this parameter to heavy REE. The $D^{S/C}$ values of moderately incompatible and moderately compatible elements (Ti, Zr, Hf, Sc, and V) are close to one. Thus, the trace elements can be divided into three groups depending on their garnet–melt partitioning. Light REE, Ba, and Sr are more soluble in silicate melts compared with $CO_2$-bearing ones; the partitioning of middle REE, Ti, Zr, Hf, Sc, V, and Ta should not change at the transition from silicate to $CO_2$-rich melts; and heavy REE and Y can be efficiently transported by $CO_2$-bearing melts (Fig. 10).

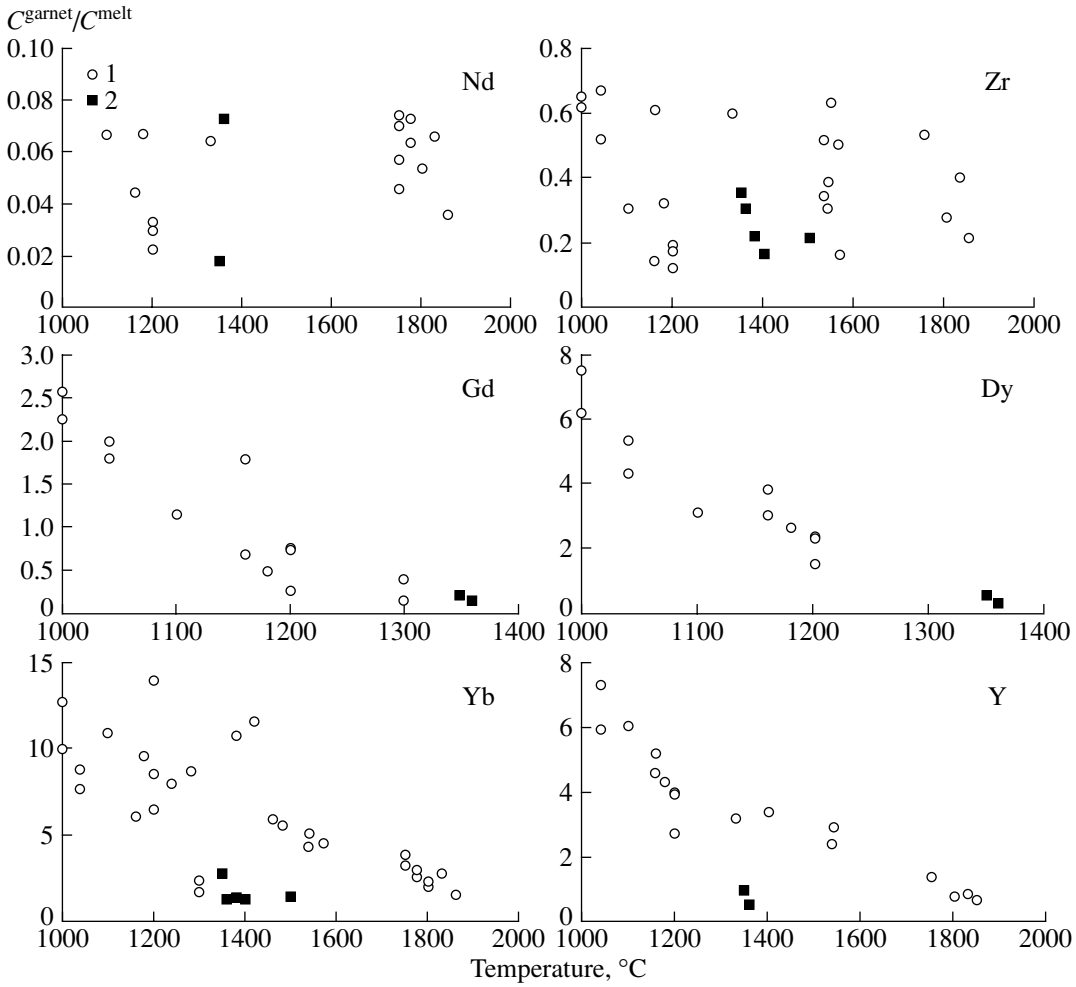


**Fig. 9.** Temperature effects on the partition coefficients of elements between (1) garnet and volatile-poor silicate melts (Barth et al., 2002; Bennett et al., 2004; Draper et al., 2003; Green et al., 2000; Nicholls and Harris, 1980; Van Westrenen et al., 1999, 2000) and (2) garnet and $CO_2$-saturated kimberlite melt (our experiments).

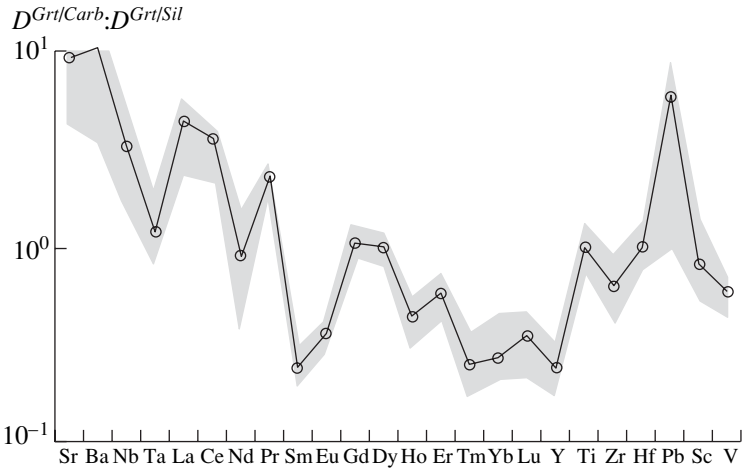


**Fig. 10.** Ratios of trace element partition coefficients between garnet and kimberlite melt ($D^{Grt/Carb}$) and between garnet and silicate melt ($D^{Grt/Sil}$) at temperatures of 1300–1450°C. The circles connected with the solid line are average values, and the shaded field shows variations in the ratio related to the uncertainty of partition coefficients for the silicate and carbonate–silicate systems.

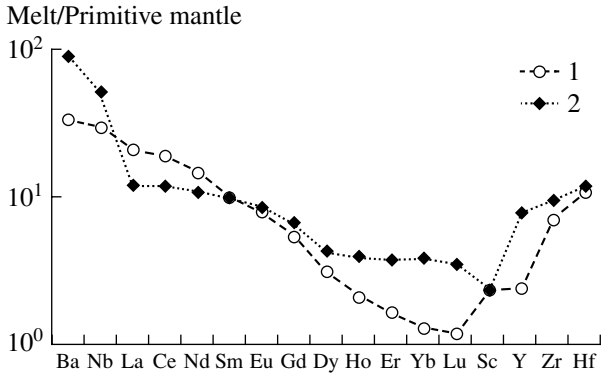


**Fig. 11.** Model compositions of basaltic melts formed by the melting of enriched (metasomatized) mantle. The initial material is represented by the primitive mantle impregnated by a small fraction (5%) of (1) silicate or (2) carbonate–silicate melt. The basaltic melts shown in the diagram are formed by 10% batch melting of the enriched mantle material.

In order to illustrate possible effects related to the presence of carbonate–silicate melts in the mantle, the formation and migration of small melt portions were numerically simulated, and the influence of these processes on the composition of subsequently derived basaltic magma was estimated. The primitive mantle was used as an initial material, in which the concentrations of all trace elements were set to 1 (which is equivalent to the normalization to primitive mantle values). The model included three stages. (1) Formation of a small portion of partial melt near the solidus of peridotite in equilibrium with a residual mantle assemblage. Taking into account the high mobility of carbonate melt (Hunter and McKenzie, 1989), the degree of melting for the carbonate melt was taken to be 0.5%, and that for the silicate melt, 2%. It was assumed that the mantle material consists of 60% olivine, 20% orthopyroxene, 10% clinopyroxene, and 10% garnet. The mineral–silicate melt partition coefficients were taken from high-pressure experimental studies (Fujimaki et al., 1984; Arth, 1976; Irving and Frey, 1978). The bulk partition coefficients between minerals and carbonate melts were determined from the values for silicate melts and $D^{S/C}$. (2) Movement of the melts and formation of enriched mantle domains composed of 95% primitive material and 5% low-degree melt. (3) Melting of the enriched mantle assuming a degree of melting of 10% and the batch melting mechanism. Such a simplified model allowed us to reveal some general relationships weakly affected by variations in physical parameters. The main distinctions between the effects produced by carbonate–silicate and silicate melts can be clearly seen in Fig. 11. In the case of mantle enrichment by carbonate–silicate melts, high concentrations of Ba and Nb are associated with relatively weakly fractionated REE distribution patterns.

The obtained results corroborate some geochemical criteria used for distinguishing the contribution of carbonate melts to mantle enrichment (Rudnick et al., 1993; Ionov et al., 1993), for instance, high Ba/La value. In contrast, strong REE fractionation (high La/Yb ratios) and high Sm/Hf and Zr/Hf ratios were not observed. Carbonate–silicate melts can evidently efficiently extract heavy REE and Y. Note also that the effects caused by the migration of silicate and carbonate–silicate melts are not very different. The dependence of the partition coefficients of many elements on temperature and melt composition additionally complicates reliable discrimination between metasomatic imprints generated by carbonate and silicate melts in the mantle (cf. Vannucci, 1998). In many cases, these effects cannot be distinguished, because there is a gradual transition from carbonate to silicate melts under mantle parameters. Nonetheless, the results obtained here allow us to search for geochemical indicators of mantle enrichment caused by the migration of carbonate–silicate melts using the compositions of igneous rocks.

According to Fig. 11, the most salient feature of mantle enrichment generated by carbonate–silicate melt compared with the effect of $CO_2$-free silicate melts is a relatively weak REE fractionation at a high degree of enrichment in the most incompatible elements (Ba and Nb). The melting of a reservoir enriched by the addition of carbonate–silicate melt produces basic magmas with high Ba/La and relatively low Ce/Yb ratios. Figure 12 shows variations in these parameters in some ocean island basalts, whose primary melts were formed at high pressures in the garnet stability field. These rocks show considerable variations in Ba/La and Ce/Yb. The Ce/Yb of all rocks is higher than the primitive mantle value, which is related to either the retention of garnet in the solid residua and/or source enrichment. The Ba/La ratio of some rocks is also much higher than the primitive mantle value. Note that such rocks often show relatively low Ce/Yb ratios (Fig. 12). The addition of small amounts of silicate melt derived from a garnet-bearing peridotite source can lead to considerable variations in the degree of REE fractionation (Fig. 12), whereas the Ba/La ratio must not change significantly, because these elements have similar incompatibilities in silicate systems. The considerable variations of Ba/La values in ocean island basalts could be related to the enrichment of mantle sources owing to the migration of carbonate–silicate melts.

### *Genesis of Kimberlite Magmas*

There is still no general consensus as to the source of kimberlite melts. The high degrees of enrichment in the most incompatible elements served as a basis for the suggestion of the enriched source of kimberlite magmas (metasomatized mantle) (Tainton and McKenzie, 1994). An alternative model assumes that initial kimberlite melts were derived from a material similar to the primitive mantle (Ringwood et al., 1992; Ryabchikov, 2003). This suggestion is based on the resemblance of

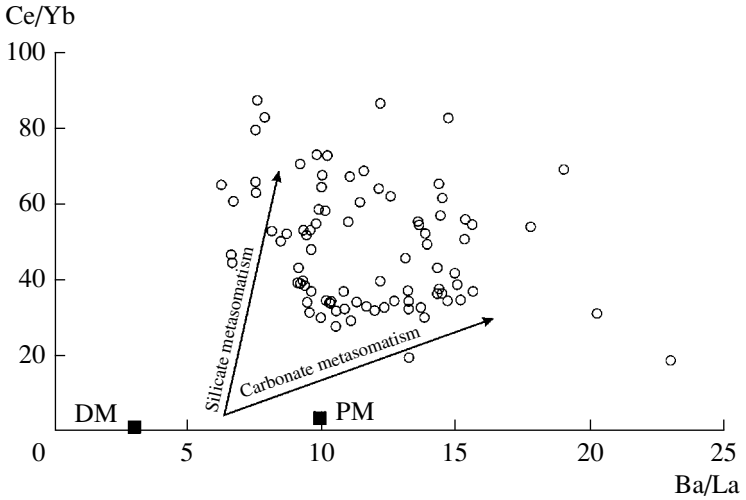


**Fig. 12.** Diagram Ce/Yb–Ba/La for selected ocean island basalts (Comores, Canaries, Cabo Verde, and Hawaii) related to mantle plume activity (Class et al., 1998; Lundstrom et al., 2003; Doucelance et al., 2003; Frey et al., 2000). The black squared indicate the compositions of the primitive mantle (PM; Palme and O'Neill, 2003) and depleted mantle (DM; Workman and Hart, 2005). The arrows show the trends of melt compositions derived from mantle sources enriched by silicate and carbonate–silicate melts.

isotopic (Ringwood et al., 1992) and trace element ratios of kimberlites to the characteristics of the primitive or slightly enriched mantle (Ryabchikov, 2003). Our results allow us to examine this problem using simple geochemical criteria.

The freshest kimberlite samples show very high light to heavy REE ratios and relatively low heavy REE contents (Tainton and McKenzie, 1994). For our analysis, we used primitive mantle-normalized (Palme and O'Neill, 2003) Yb concentrations ($Yb_n$ in kimberlites is 2.5–4.5) and $(Ce/Yb)_n$ ratios (100–200 in kimberlites) (Tainton and McKenzie, 1994). Such compositions can be generated by low-degree melting of a garnet-bearing mantle source. The maximum light REE enrichment of the melt is reached when the degree of melting approaches zero; in such a case $C_m = C_0/D$, where $C_m$ is the concentration in the melt, $C_0$ is the concentration in the source, and $D$ is the bulk partition coefficient. As can be seen in Fig. 13, even at the lowest degrees of melting of the primitive mantle, the $(Ce/Yb)_n$ ratios of carbonate–silicate melts are much lower than the kimberlite values. This implies that the single-stage melting of the primitive mantle does not provide the desired degree of REE fractionation. This circumstance served as a basis for the two-stage models of kimberlite genesis with preliminary enrichment of the source material in incompatible elements (Wyllie, 1987; Ryabchikov, 1995; Tainton and McKenzie, 1994).

It was assumed that kimberlite melts were derived from the depleted material of the continental lithospheric mantle, which was preliminarily enriched by the addition of small portions of melts from deep mantle zones (Wyllie, 1979; Eggler, 1979). Experimental studies of high-magnesium kimberlitic melts (Girnis et al., 1995) showed that their source material was probably represented by garnet harzburgite. The compositions of mantle nodules suggest that the garnet peridotites of the lithospheric mantle are relatively enriched in light REE and have low contents of heavy REE: $(Ce/Yb)_n = 8.75$ and $Yb_n = 0.8$ (McDonough, 1990).

The melting of such an enriched garnet harzburgite (composed of 75% *Ol* + 15% *Opx* + 10% *Grt*) produces near-solidus melts with high $(Ce/Yb)_n$ ratios (up to 80). In addition to the initial enrichment of the source, this effect is strengthened by the absence of residual clinopyroxene, which is the main repository of light REE in the primitive mantle. However, even in this case, the compositions of melts remain beyond the kimberlite field [$(Ce/Yb)_n > 100$] (Fig. 13). Consequently, the lithospheric peridotites need to be additionally enriched compared with the average composition. Calculations showed that melts with the desired degree of light REE enrichment can be derived from a garnet harzburgite with $(Ce/Yb)_n = 20$ and $Yb_n = 0.9$ (Fig. 13). Such compositions can be generated by the addition of a few percent of enriched carbonate–silicate melt to garnet harzburgite corresponding in the degree of REE fractionation to the average composition of garnet peridotites from the continental lithospheric mantle (McDonough, 1990).

Thus, the favored model of kimberlite magma formation includes the injection of enriched melts into the harzburgites of the lower parts of the lithospheric mantle. There are various possible variants of such a model. Carbonate melts from deep mantle levels could crystallize in such zones forming strongly enriched carbonated domains in the mantle. The formation of kimberlites could be related to the partial melting of such domains during a later heating event not related to the injection of carbonate melts. On the other hand, the injection of carbonate melts, heating, and melting of the enriched material could occur simultaneously. In such

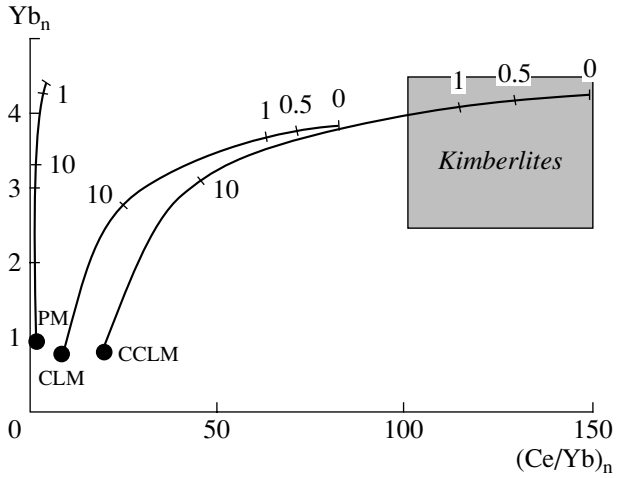


**Fig. 13.** Geochemical model for the formation of primary kimberlite melts with very high $(Ce/Yb)_n$ ratios and moderate concentrations of $Yb_n$ (Tainton and McKenzie, 1994). Variations in the composition of carbonate–silicate melts near the solidus of mantle peridotite are shown by lines. PM is the primitive mantle, and its melting produces liquids with relatively low Ce/Yb ratios; CLM is the average composition of garnet peridotites from the continental lithospheric mantle (McDonough, 1990), and melts obtained from this reservoir may show very fractionated REE distribution patterns, but the maximum Ce/Yb value is lower than that of kimberlites; CCLM is the carbonated lithospheric mantle additionally enriched by the addition of 3% carbonate melt, the near-solidus melt from this source fall within the field of kimberlites. The numbers near the lines denote the degree of melting of the sources in weight percent.

a case, kimberlites can be considered as products of interaction between deep asthenospheric magmas (Ringwood et al., 1992) with moderately enriched garnet harzburgites in the deep zones of the lithospheric mantle (Girnis et al., 1995). The latter scenario seems to be more plausible, because it explains why the isotopic characteristics of kimberlites correspond to those of asthenospheric mantle sources (Smith et al., 1985).

## CONCLUSIONS

Although the content of carbon in the primitive mantle is relatively low (about 100 ppm; Palme and O'Neill, 2003), the high incompatibility of $CO_2$ in the mantle (if carbonates are absent) causes the formation of carbonate melts during the early stages of melting of mantle peridotites. The considerable temperature interval between the solidi of "dry" and $CO_2$-bearing peridotite (Dalton and Presnall, 1998) indicates that carbonate–silicate melts may be widespread in the mantle. The high mobility of such liquids (Hunter and McKenzie, 1989) makes them a possible agent of mantle metasomatism. There is little direct evidence for the movement of small portions of carbonate melt in mantle rocks (e.g., Ionov et al., 1993, 1996; Frezzotti et al., 2002), which can be explained by the occurrence of decarbonation reactions during decompression. Therefore, the geochemical systematics of basic magmas is the main source of information on the character of carbonate metasomatism (Ionov et al., 1993; Rudnick et al., 1993). Experimental data on trace element partitioning between mantle minerals and melts provide a necessary basis for the modeling of mass transfer processes in the mantle. The results obtained in this study characterize the behavior of elements under relatively high-temperature conditions, when near-solidus mantle magmas are essentially anhydrous. Such conditions can be created during the melting of mantle peridotites that experienced a previous stage of depletion in incompatible elements, including water. A comparison of our data with the published experiments for carbonate and silicate systems showed that the partition coefficients of trace elements in mantle systems are not constant. This is especially important for moderately incompatible and compatible elements (heavy REE, Zr, Y, etc.), the behavior of which is strongly dependent on temperature and melt composition. Hence, any modeling of mantle metasomatism and interpretation of geochemical data must take into account not only the character of metasomatic agents (carbonate melt, silicate melt, or aqueous fluid) but also thermodynamic conditions. The application of this approach to kimberlite magmas showed that they could be formed by the melting of depleted mantle material that had been pre-enriched by the injection of small portions of carbonate or carbonate–silicate melts.

## ACKNOWLEDGMENTS

The authors are grateful to I.P. Solovova and I.T. Rass (Institute of Geology of Ore Deposits, Petrography, Mineralogy, and Geochemistry, Russian Academy of Sciences) for their careful reading of the manuscript and helpful comments. This study was financially supported by the Deutsche Forschungsgemeinschaft (DFG), Russian Foundation for Basic Research (project nos. 05-05-64175 and 04-05-64830), and the Program for the Support of Leading Scientific Schools.

## REFERENCES

1. J. Adam and T. Green, "Experimentally Determined Partition Coefficients for Minor and Trace Elements in Peridotite Minerals and Carbonatitic Melt, and Their Relevance to Natural Carbonatites," Eur. J. Mineral. **13**, 815–827 (2001).
2. J. G. Arth, "Behavior of Trace Elements during Magmatic Processes—A Summary of Theoretical Models and Their Applications," J. Res. US Geol. Surv. **4**, 41–47 (1976).
3. M. G. Barth, S. F. Foley, and I. Horn, "Partial Melting in Archean Subduction Zones: Constraints from Experimentally Determined Trace Element Partition Coefficients between Eclogitic Minerals and Tonalitic Melts under Upper Mantle Conditions," Precambrian Res. **113**, 323–340 (2002).

4. S. L. Bennett, J. Blundy, and T. Elliott, "The Effect of Sodium and Titanium on Crystal–Melt Partitioning of Trace Elements," Geochim. Cosmochim. Acta **68**, 2335–2347 (2004).
5. J. Blundy and J. Dalton, "Experimental Comparison of Trace Element Partitioning between Clinopyroxene and Melt in Carbonate and Silicate Systems, and Implications for Mantle Metasomatism," Contrib. Mineral. Petrol. **139**, 356–371 (2000).
6. G. P. Brey, R. Weber, and K. G. Nickel, "Calibration of a Belt Apparatus to 1800°C and 6 GPa," J. Geophys. Res. **95**, 15603–15610 (1990).
7. C. Class, S. Goldstein, R. Altherr, and P. Bachelery, "The Process of Plume–Lithosphere Interactions in the Ocean Basins—The Case of Grand Comore," J. Petrol. **39**, 881–903 (1998).
8. J. A. Dalton and D. C. Presnall, "Carbonatitic Melts along the Solidus of Model Lherzolite in the System $CaO–MgO–Al_2O_3–SiO_2–CO_2$ from 3 to 7 GPa," Contrib. Mineral. Petrol. **131**, 123–135 (1998).
9. J. A. Dalton and B. J. Wood, "The Compositions of Primary Carbonate Melts and Their Evolution through Wallrock Reaction in the Mantle," Earth Planet. Sci. Lett. **119**, 511–525 (1993).
10. R. Doucelance, S. Escrig, M. Moreira, et al., "Pb–Sr–He Isotope and Trace Element Geochemistry of the Cape Verde Archipelago," Geochim. Cosmochim. Acta. **67**, 3717–3733 (2003).
11. D. S. Draper, D. Xirouchakis, and C. B. Agee, "Trace Element Partitioning between Garnet and Chondritic Melt from 5 to 9 GPa: Implications for the Onset of the Majorite Transition in the Martian Mantle," Phys. Earth Planet. Int. **139**, 149–169 (2003).
12. D. H. Eggler, "Kimberlites: How Do They Form?" in *Kimberlites and Related Rocks*, Ed. by J. Ross et al. (Blackwell, Melbourne, 1989), Vol. 1, pp. 489–504.
13. F. A. Frey, D. Clague, J. J. Mahoney, and J. M. Sinton, "Volcanism at the Edge of the Hawaiian Plume: Petrogenesis of Submarine Alkalic Lavas from the North Arch Volcanic Field," J. Petrol. **41**, 667–691 (2000).
14. M.-L. Frezzotti, J. L. R. Touret, and E.-R. Neumann, "Ephemeral Carbonate Melts in the Upper Mantle: Carbonate–Silicate Immiscibility in Microveins and Inclusions within Spinel Peridotite Xenoliths, La Gomera, Canary Islands," Eur. J. Mineral. **14**, 891–904 (2002).
15. H. Fujimaki, M. Tatsumoto, and K.-I. Aoki, "Partition Coefficients of Hf, Zr, and REE between Phenocrysts and Groundmasses," J. Geophys. Res. **89**, 662–672 (1984).
16. A. V. Girnis, G. P. Brey, and I. D. Ryabchikov, "Origin of Group IA Kimberlites: Fluid Saturated Melting Experiments at 45–55 kbar," Earth Planet. Sci. Lett. **134**, 283–296 (1995).
17. A. V. Girnis, V. K. Bulatov, and G. P. Brey, "Transition from Kimberlite to Carbonatite Melt under Mantle Parameters: An Experimental Study," Petrologiya **13**, 3–18 (2005) [Petrology **13**, 1–15 (2005)].
18. D. H. Green and M. E. Wallace, "Mantle Metasomatism by Ephemeral Carbonatite Melts," Nature **336**, 459–462 (1988).
19. T. H. Green, J. D. Blundy, J. Adam, and G. M. Yaxley, "SIMS Determination of Trace Element Partition Coefficients between Garnet, Clinopyroxene and Hydrous Basaltic Liquids at 2–7.5 GPa and 1080–1200°C," Lithos **53**, 165–187 (2000).
20. R. H. Hunter and D. McKenzie, "The Equilibrium Geometry of Carbonate Melts in Rocks of Mantle Composition," Earth Planet. Sci. Lett. **92**, 347–356 (1989).
21. D. A. Ionov, C. Dupuy, S. Y. O'Reilly, et al., "Carbonated Peridotite Xenoliths from Spitsbergen: Implications for Trace Element Signature of Mantle Carbonate Metasomatism," Earth Planet. Sci. Lett. **119**, 283–297 (1993).
22. D. A. Ionov, S. Y. O'Reilly, Yu. S. Genshaft, and M. G. Kopylova, "Carbonate-Bearing Mantle Peridotite Xenoliths from Spitsbergen: Phase Relationships, Mineral Compositions and Trace-Element Residence," Contrib. Mineral. Petrol. **125**, 375–392 (1996).
23. A. J. Irving and F. A. Frey, "Distribution of Trace Elements between Garnet Megacrysts and Host Volcanic Liquids of Kimberlitic to Rhyolitic Composition," Geochim. Cosmochim. Acta. **42**, 771–787 (1978).
24. S. Keshav, A. Corgne, G. H. Gudfinnsson, et al., "Kimberlite Petrogenesis: Insights from Clinopyroxene–Melt Partitioning Experiments at 6 GPa in the $CaO–MgO–Al_2O_3–SiO_2–CO_2$ System," Geochim. Cosmochim. Acta **69**, 2829–2845 (2005).
25. S. Klemme and C. Dalpe, "Trace-Element Partitioning between Apatite and Carbonatite Melt," Am. Mineral. **88**, 639–646 (2003).
26. S. Klemme, S. R. van der Laan, S. F. Foley, and D. Gunther, "Experimentally Determined Trace and Minor Element Partitioning between Clinopyroxene and Carbonatite Melt under Upper Mantle Conditions," Earth Planet. Sci. Lett. **133**, 439–448 (1995).
27. Y. Lahaye, D. Lambert, and S. Walters, "Ultraviolet Laser Sampling and High-Resolution Inductively Coupled Plasma Mass Spectrometry of NIST and BCR-2G Glass Reference Materials," Geostand. Newslett. **21**, 205–214 (1997).
28. C. C. Lundstrom, K. Hoernle, and J. Gill, "U-Series Disequilibria in Volcanic Rocks from the Canary Islands: Plume versus Lithospheric Melting," Geochim. Cosmochim. Acta. **67**, 4153–4177 (2003).
29. W. F. McDonough, "Constraints on the Composition of the Continental Lithospheric Mantle," Earth Planet. Sci. Lett. **101**, 1–18 (1990).
30. K. R. Moore and B. J. Wood, "The Transition from Carbonate to Silicate Melts in the $CaO–MgO–SiO_2–CO_2$ System," J. Petrol. **39**, 1943–1951 (1998).
31. I. A. Nicholls and K. L. Harris, "Experimental Rare Earth Element Partition Coefficients for Garnet, Clinopyroxene and Amphibole Coexisting with Andesitic and Basaltic Liquids," Geochim. Cosmochim. Acta **44**, 287–308 (1980).
32. K. G. Nickel and G. P. Brey, "Subsolidus Orthopyroxene–Clinopyroxene Systematics in the System $CaO–MgO–SiO_2$ to 60 kb: A Re-Evaluation of the Regular Solution Model," Contrib. Mineral. Petrol. **87**, 35–42 (1984).
33. H. Palme and H. St. C. O'Neill, "Cosmochemical Estimates of Mantle Composition," in *Treatise on Geochemistry* (Elsevier, Amsterdam, 2003), Vol. 2, pp. 1–38.

34. A. E. Ringwood, S. E. Kesson, W. Hibberson, and N. Ware, "Origin of Kimberlites and Related Magmas," Earth Planet. Sci. Lett. **113**, 521–538 (1992).

35. R. Rudnick, W. F. McDonough, and B. C. Chappell, "Carbonatite Metasomatism in the Northern Tanzanian Mantle," Earth Planet. Sci. Lett. **114**, 463–475 (1993).

36. I. D. Ryabchikov, "Geochemical Model of the Generation of Kimberlitic Melts," Geochem. Int. **32**, 103–111 (1995).

37. I. D. Ryabchikov, "Mechanisms and Conditions of Magma Formation in Mantle Plumes," Petrologiya **11**, 548–555 (2003) [Petrology **11**, 496–503 (2003)].

38. I. D. Ryabchikov, G. Brey, L. N. Kogarko, and V. K. Bulatov, "Partial Melting of Carbonated Peridotite at 50 kbar," Geokhimiya, No. 1, 3–9 (1989).

39. I. D. Ryabchikov, G. Brey, and V. K. Bulatov, "Carbonate Melts in Equilibrium with Mantle Peridotite at 50 kbar," Petrologiya **1**, 189–194 (1993).

40. C. B. Smith, J. J. Gurney, E. M. W. Skinner, et al., "Geochemical Character of Southern African Kimberlites: A New Approach Based on Isotopic Constraints," Trans. Geol. Soc. S. Afr. **88**, 267–280 (1985).

41. R. J. Sweeney, "Carbonatite Melt Compositions in the Earth's Mantle," Earth Planet. Sci. Lett. **128**, 259–270 (1994).

42. R. J. Sweeney, D. H. Green, and S. H. Sie, "Trace and Minor Element Partitioning between Garnet and Amphibole and Carbonatitic Melt," Earth Planet. Sci. Lett. **113**, 1–14 (1992).

43. R. J. Sweeney, V. Prozesky, and W. Przybylowicz, "Selected Trace and Minor Element Partitioning between Peridotite Minerals and Carbonatite Melts at 18-46 kb Pressure," Geochim. Cosmochim. Acta **59**, 3671–3683 (1995).

44. K. M. Tainton and D. McKenzie, "The Generation of Kimberlites, Lamproites, and Their Source Rocks," J. Petrol. **35**, 787–817 (1994).

45. W. Van Westrenen, J. Blundy, and B. Wood, "Crystal-Chemical Controls on Trace Element Partitioning between Garnet and Anhydrous Silicate Melt," Am. Mineral. **84**, 838–847 (1999).

46. W. Van Westrenen, J. D. Blundy, and B. J. Wood, "Effect of $Fe^{2+}$ on Garnet–Melt Trace Element Partitioning: Experiments in FCMAS and Quantification of Crystal-Chemical Controls in Natural Systems," Lithos **53**, 189–201 (2000).

47. R. Vannucci, P. Bottazzi, E. Wulff-Pedersen, and E.-R. Neumann, "Partitioning of REE, Y, Sr, Zr and Ti between Clinopyroxene and Silicate Melts in the Mantle under Palma (Canary Islands): Implications for the Nature of the Metasomatic Agents," Earth Planet. Sci. Lett. **158**, 39–51 (1998).

48. M. E. Wallace and D. H. Green, "An Experimental Determination of Primary Carbonatite Magma Composition," Nature **335**, 343–346 (1988).

49. R. K. Workman and S. R. Hart, "Major and Trace Element Composition of the Depleted MORB Mantle (DMM)," Earth Planet. Sci. Lett. **231**, 53–72 (2005).

50. P. J. Wyllie, "Kimberlite Magmas from the System Peridotite–$CO_2$–$H_2O$," in *"Kimberlites, Diatremes, and Diamonds: Their Geology, Petrology and Geochemistry,"* Ed. by F. R. Boyd and H. O. A. Meyer (Am. Geophys. Un., Washington, DC, 1979), pp. 319–329.

51. P. J. Wyllie, "Discussion of Recent Papers on Carbonated Peridotite, Bearing on Mantle Metasomatism and Magmatism," Earth Planet. Sci. Lett. **82**, 391–397 (1987).

52. P. J. Wyllie, "The Genesis of Kimberlites and Some Low-$SiO_2$, High-Alkali Magmas," in *Kimberlites and Related Rocks*, Ed. by J. Ross et al. (Blackwell, Melbourne, 1989), pp. 605–615.

53. G. M. Yaxley and D. H. Green, "Experimental Reconstruction of Sodic Dolomitic Carbonatite Melts from Metasomatised Lithosphere," Contrib. Mineral. Petrol. **124**, 359–369 (1996).

54. G. M. Yaxley, A. J. Crawford, and D. H. Green, "Evidence for Carbonatite Metasomatism in Spinel Peridotite Xenoliths from Western Victoria, Australia," Earth Planet. Sci. Lett. **107**, 305–317 (1991).